

Fourier Basis Mapping: A Time-Frequency Learning Framework for Time Series Forecasting

Runze Yang¹, Longbing Cao², Xin You³, Kun Fang⁴, Jianxun Li⁵, Jie Yang⁶

Abstract—The integration of Fourier transform and deep learning opens new avenues for time series forecasting. We reconsider the Fourier transform from a basis functions perspective. Specifically, the real and imaginary parts of the frequency components can be regarded as the coefficients of cosine and sine basis functions at tiered frequency levels, respectively. We find that existing Fourier-based methods face inconsistent starting cycles and inconsistent series length issues. They fail to interpret frequency components precisely and overlook temporal information. Accordingly, the novel Fourier Basis Mapping (FBM) method addresses these issues by integrating time-frequency features through Fourier basis expansion and mapping in the time-frequency space. Our approach extracts explicit frequency features while preserving temporal characteristics. FBM supports plug-and-play integration with various types of neural networks by only adjusting the first initial projection layer for better performance. First, we propose FBM-L, FBM-NL, and FBM-NP to enhance linear, MLP-based, and Transformer-based models, respectively, demonstrating the effectiveness of time-frequency features. Next, we propose a synergetic model architecture, termed FBM-S, which decomposes the seasonal, trend, and interaction effects into three separate blocks, each designed to model time-frequency features in a specialized manner. Finally, we introduce several techniques tailored for time-frequency features, including interaction masking, centralization, patching, rolling window projection, and multi-scale down-sampling. The results are validated on diverse real-world datasets for both long-term and short-term forecasting tasks with SOTA performance.

Index Terms—Time Series Forecasting, Fourier Basis Mapping, Time-Frequency Features, Deep Neural Network

I. INTRODUCTION

TIME series forecasting (TSF) plays a vital role across a wide range of industries, including energy, weather prediction, financial markets, and transportation systems. For example, time series forecasting is crucial for forecasting weather to support disaster readiness, predicting financial market movements to inform investment strategies and policymaking, and estimating traffic flow to aid in urban planning and optimize transportation systems. However, it faces considerable challenges, such as modeling both short-term

and long-term temporal dependencies, along with frequency-oriented global dynamics. Recently, deep neural networks (DNNs) have thrived to tackle TSF challenges for the presence of hierarchical effects, varied outliers, and nonlinear dynamics. They use various DNN architectures including recurrent neural networks (RNNs) [1]–[9], convolution neural networks (CNNs) [10]–[16], multi-layer perceptron (MLP)-based networks [17]–[22], Transformer-based networks [23]–[39] and graph neural networks (GNNs) [40]–[44] and Mamba-based networks [45]–[47]. Interestingly, the recent NLinear study [48] demonstrates that a surprisingly simple normalized linear model can surpass the performance of most deep neural network (DNN)-based approaches. This raises the question: *Would a complex DNN architecture necessarily lead to better TSF performance?* According to CrossGNN [40], DNN-based methods are susceptible to noisy inputs, often assigning high attention scores or weights to irrelevant or unexpected signals.

Thus, Fourier-based time series modeling emerges as a new paradigm to remove noise signals by decomposing diverse effects hierarchically at different frequency levels. If we rethink the Fourier transform from a basis functions perspective, the real and imaginary parts can be interpreted as the coefficients of cosine and sine basis functions at tiered frequencies, respectively. However, existing Fourier-based methods do not involve basis functions, thus failing to interpret frequency coefficients sufficiently. They face two main issues: inconsistent starting cycles and inconsistent series length issues, as detailed in Section III. For instance, FEDformer [39], FreTS [22], FiLM [9], FITS [49], FGNet [31], and FL-Net [50] use the real and imaginary parts of frequency components as input and conduct the mapping in the frequency space. From our new perspective, we find that the amplitude and arctangent of the real and imaginary components carry more explicit meanings than the components themselves, as adding a cosine wave and a sine wave with the same frequency leads to a shifted cosine wave with the same frequency and a fused amplitude. Furthermore, the meanings of frequency components are bounded by the series length, and overlooking this causes ambiguity in interpreting precise frequencies in these models. For example, a k Hz sine or cosine wave can have different meanings depending on the series length. More importantly, Figure 1 shows that a Fourier basis function is time-dependent when the input length is not divisible by the frequency level, making it even more challenging for the model to accurately interpret those frequency components without the basis functions. Existing methods receive these coefficients unaware they correspond to specific sine and cosine basis functions. Consequently,

R. Yang is with the Department of Automation, Shanghai Jiao Tong University, Shanghai, China, and the School of Computing, Macquarie University, Sydney, Australia (e-mails: runze.y@sjtu.edu.cn, runze.yang@mq.hdr.edu.au). L. Cao is with the School of Computing, Macquarie University, Sydney, Australia (e-mail: longbing.cao@mq.edu.au). X. You, J. Yang and J. Li are with the Department of Automation, Shanghai Jiao Tong University, Shanghai, China (e-mails: {sjtu_youxin, jieyang, lijx}@sjtu.edu.cn). Kun Fang is with the department of Electrical and Electronic Engineering, Hong Kong Polytechnic University, Hong Kong, China. (e-mails: kun.fang@polyu.edu.hk). This research is partially supported by NSFC (No. 62376153), and ARC DP240102050 and LE240100131. Corresponding authors: L. Cao and J. Yang. The project is online at: <https://github.com/runze1223/FBM-S>

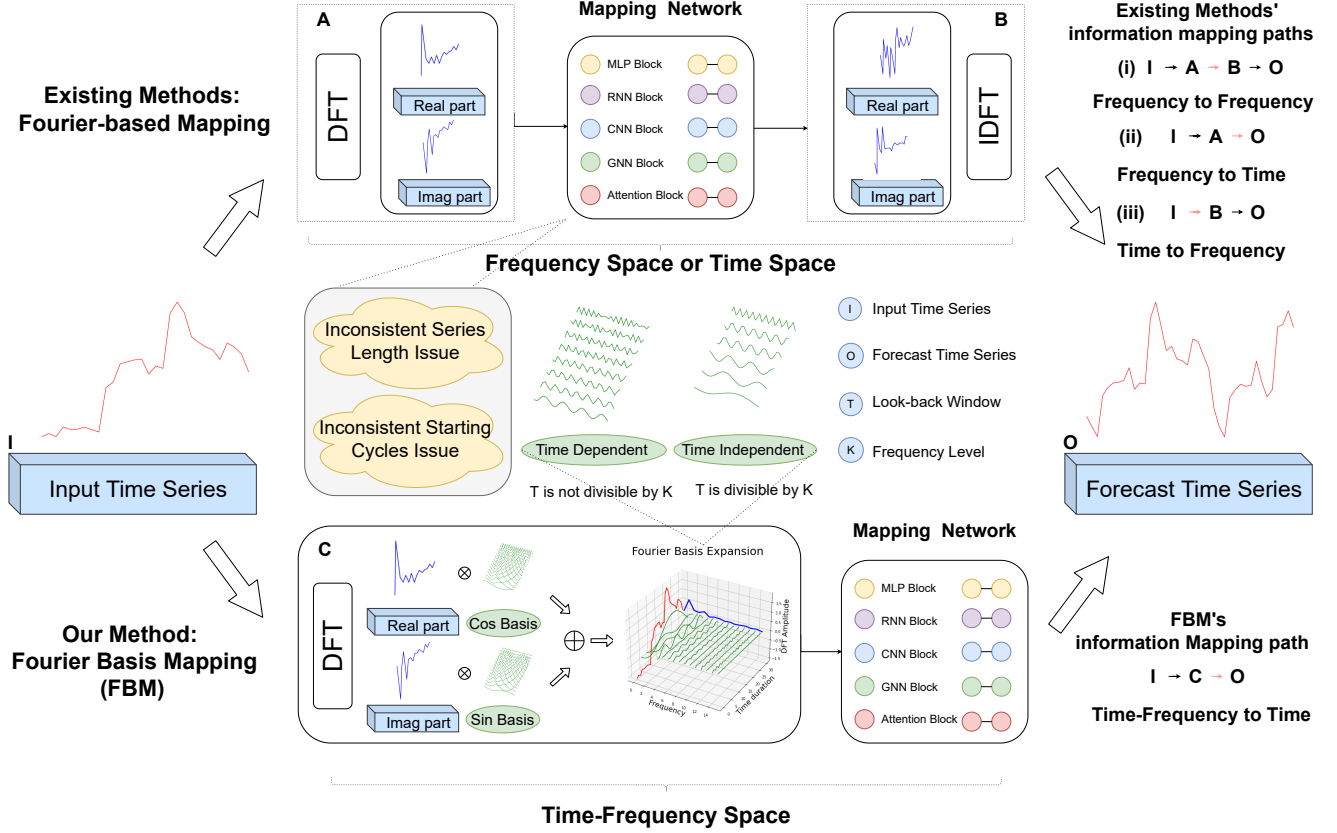


Fig. 1: Comparison of Existing Fourier-based Methods with Our Approach Fourier basis mapping. Existing methods primarily operate in the frequency space or time space, with the mapping focusing on frequency or time features. Our FBM simultaneously operates in time-frequency space, with the mapping focusing on time-frequency features.

constructing the mapping in the frequency space is not enough and neglect temporal information, which has been ignored by existing Fourier-based methods. Although some methods like TimesNet [16] consider both time and frequency features, these features are non-interpretable and complex because they are extracted by deep layers, and summation over the frequency dimension does not recover the original time series. We provide a more detailed discussion of their limitations in Section II.

Accordingly, we propose Fourier Basis Mapping (FBM) to address the aforementioned issues by incorporating Fourier basis functions, enabling the model to capture more explicit frequency information while preserving temporal characteristics. In Figure 1, we visualize the difference between our method and existing Fourier-based methods. In the first stage, we embed the discrete Fourier transform with basis functions, referred to as *Fourier basis expansion*, to extract time-frequency features. In the second stage, we map the time-frequency features into output time series. As our time-frequency features retain time domain information, thus it can be applied to any time-based mapping methods, by only adjusting the first initial projection layer but considering both time and frequency modality. Firstly, we validate the effectiveness of incorporating time-frequency features into three types of mapping networks, resulting in three FBM variants: FBM-L, FBM-NL, and FBM-NP. This demonstrate that Fourier basis expansion can en-

hance any type of DNNs, serving as a plug-and-play module. With time-frequency features, even simple mapping networks (e.g., L-vanilla linear networks and NL-three-layer MLPs) can achieve very good performance. Secondly, we propose a synergetic FBM model, referred to as FBM-S, investigating how to model time-frequency features more efficiently and effectively. The model decomposes seasonal, trend, and interaction effects into three separate blocks, each of which models the time-frequency features in a specialized manner. Our method highlights that separating endogenous and exogenous effects into separate blocks is crucial. Existing studies either use independent channels or dependent channels but fail to combine the strengths of both effectively. This is because they overlook the fact that inference between multivariate time series usually occurs over short-term periods. Therefore, input and output masks are applied to the interaction blocks to enable smoother integration of their respective strengths. Finally, we introduce several techniques tailored for time-frequency features within each block, including masking and centralization in the interaction block, patching, centralization and multi-scale down-sampling in the trend block, and rolling window projections in the seasonal block.

The proposed FBM variants are compared against six categories of TSF baseline methods: (1) Linear method; (2) Transformer-based methods; (3) MLP-based methods; (4) RNNs-based methods; (5) CNNs-based methods; and (6)

Fourier-based methods. Evaluations are conducted on diverse datasets for both long-term and short-term forecasting tasks with SOTA performance.

Our main contributions include the following:

- We identify two issues in existing Fourier-based methods: inconsistent starting cycles issue and inconsistent series lengths issue.
- We introduce the Fourier Basis Mapping (FBM) framework to extract explicit time-frequency features, addressing the aforementioned issues by mapping within the time-frequency space.
- We demonstrate that our method supports plug-and-play integration with various types of neural networks to enhance performance, as validated by three proposed FBM variants: FBM-L, FBM-NL, and FBM-NP.
- We propose FBM-S, a synergetic FBM model that efficiently captures time-frequency relationships by decomposing effects into trend, seasonal, and interaction components within three specialized blocks, incorporating several useful techniques for time-frequency features.

This study is an extension of its conference version [51]. In the conference version, we first point out the inconsistent starting cycles and series length issues, and demonstrated the effectiveness of the proposed time-frequency through plug-and-play in the existing methods, primary focusing on the long-term TSF task. In the extension version, we further investigate how to use time-frequency features more effectively and efficiently, and create our own architecture, a synergetic FBM model, tailored for time-frequency mapping, focusing on both the long-term and short-term TSF tasks.

The main differences in this extended version are as follows: (i) We revise the workflow of the introduction and related work to reflect the new motivations mentioned above. (ii) We propose a new synergistic FBM model, termed FBM-S, which applies trend, seasonal, and interaction decomposition along with several techniques tailored for time-frequency features, as detailed in Section IV-C. (iii) In Section V, we add experimental settings for short-term TSF with more diverse prediction lengths on the PEMS dataset and include a new dataset M4. (iv) We completely rewrite Section VI, with a summary provided in Section VI-A. In Section VI, except for some parts of the long-term TSF results that are retained, all other content, including short-term TSF results, efficiency analysis, ablation studies, visualizations, and case studies, is newly added for FBM-S to support the broader scope of this extended version.

II. RELATED WORK

Recent research has highlighted the potential of the Fourier transform in addressing challenges in time series forecasting (TSF). Accordingly, we categorize the relevant work into two groups: (1) frequency-based methods and (2) time-based methods. We discuss the unique strengths and weaknesses of each approach and explain how our method is designed to overcome their limitations and complement their strengths.

A. Frequency-based Methods

Fourier transform has been integrated into a wide range of network architectures, including RNNs [9], CNNs [16], MLP-based networks [20]–[22], Transformer-based networks [38], [39], and graph neural networks (GNNs) [40], [41]. However, by rethinking the Fourier transform from a basis functions perspective, we identify the inconsistent starting cycles and series length issues. In path (i) of Figure 1, methods like FEDformer [39], FreTS [22], FiLM [9], FITS [49], FGNet [31], and FL-Net [50] use real and imaginary parts as inputs and conduct the mapping in a frequency space but the networks cannot easily interpret those coefficients because crucial information is stored in the amplitude, phase and length of each cycle. In path (ii) of Figure 1, methods such as CrossGNN [40] use the discrete Fourier transform (DFT) to select the top k amplitudes for noise filtering, retaining only the first cycle and neglecting the phase shift, along with the fact that the basis functions can become time dependent when the frequency is not divisible by the series length. However, a higher amplitude does not necessarily indicate a useful frequency, and a lower amplitude is not necessarily useless. TimesNet [16] introduce the multi-window Fourier transform. However, their approach lacks mathematical rigor and their model architecture is both complex and inefficient, as the original time-domain information has been compromised. In path (iii) of Figure 1, methods such as N-BEATS [20] and N-Hits [21] can similarly be viewed as forecasting through the inverse discrete Fourier transform (IDFT) by computing the output frequency spectrum of the time series, but their networks struggle to capture time-dependent effects and do not leverage frequency information effectively. In contrast, our method distinguishes itself from existing approaches by leveraging the Fourier basis expansion to provide a mixture of time-frequency features, thus avoiding the aforementioned issues.

B. Time-based Methods

The popular time-based architectures involve RNNs [1]–[8], CNNs [10]–[15], MLP-based networks [17]–[19], Transformer-based methods [23]–[37], and graph neural networks (GNNs) [42]–[44]. Among Transformer-based models for time series forecasting, PatchTST [24] and iTransformer [35] have emerged as two of the most influential architectures for independent and dependent modeling, respectively. PatchTST introduces patching by treating a segment of local time points as a semantic vector and models each channel independently. In contrast, iTransformer reverses the traditional Transformer structure by embedding each time series as a variate token, using the attention mechanism to capture inter-variates relationships. Meanwhile, the approach of embedding multivariate time series into a single token for each time point, as adopted by models such as LogTrans [52], Pyraformer [28], Informer [26], and Autoformer [27], has become less popular in recent years. We find that independent channel modeling is more suitable for capturing endogenous temporal relationships within each time series, while interaction modeling is better at capturing exogenous relationships between multivariate time

series. These two aspects can be complemented and studied separated; however, there has been no effective investigation into combining them, as prior work has not recognized that interaction effects typically occur only over short time periods. To address this, we propose a masking mechanism in our research. Finally, we discuss several techniques that are useful for time-based mapping networks. VH-NBEATS [53] incorporates pre-trained basis functions to capture hourly, daily, and weekly effects, which is particularly effective for long-term TSF and low-granularity data. Autoformer [27] advocates trend and seasonal decomposition with the moving average kernel, consistent with other methods such as DLinear [48]. However, the effectiveness of decomposition is based on the choice of kernel size, which is improved by our methods. In [54], standardization and centralization are introduced in time domain to enhance the robustness. TimeMixer [17] introduces a multi-resolution downsampling strategy to study different effects. However, the effectiveness of these techniques for mapping time-frequency features has not yet been studied. In this work, we develop similar techniques tailored for time-frequency representations.

In conclusion, time-based methods lack a global perspective of time series but facilitate the capture of fine-grained temporal relationships. In contrast, frequency-domain-based mapping offers a global view and supports the decomposition of various effects, but it loses important temporal details. Therefore, we introduce a time-frequency learning framework that leverages Fourier basis expansion to extract time-frequency features, effectively combining the strengths of both domains.

III. RETHINKING FOURIER TRANSFORM W.R.T. BASIS FUNCTIONS

In this section, we present a new perspective of the Fourier transform for TSF. First, we discuss the mathematical reasoning behind the DFT and IDFT in terms of basis functions. From this new basis perspective, we observe that the real and imaginary parts of the frequency components correspond to the coefficients of cosine and sine basis functions across different frequency levels. As such, we identify inconsistent starting cycles and inconsistent series length issues in existing studies.

Let \mathbf{X} and \mathbf{Y} represent the input and output time series, respectively, and T and L refer to the look-back window and forecast horizon, both assumed to be even numbers. \mathbf{H}^X and \mathbf{H}^Y denote the frequency spectrum of the input and output, respectively. Then, DFT and IDFT of the input time series \mathbf{X} can be expressed as follows:

$$\begin{aligned} \mathbf{H}(k) &= DFT(\mathbf{X}) = \sum_{n=0}^{T-1} \mathbf{X}[n] \exp\left(-i \frac{2\pi kn}{T}\right), \\ \mathbf{X}[n] &= IDFT(\mathbf{H}) = \frac{1}{T} \sum_{k=0}^{T-1} \mathbf{H}[k] \exp\left(i \frac{2\pi kn}{T}\right), \end{aligned} \quad (1)$$

$$n = 0, 1, \dots, T-1, \quad k = 0, 1, \dots, T-1$$

From the perspective of basis functions, IDFT can be expressed by $\frac{T}{2}+1$ orthogonal cosine basis functions and $\frac{T}{2}-1$ orthogonal sine basis functions. This is because the frequency components of a real-valued signal are Hermitian symmetric.

The proof can be found in Appendix A. Subsequently, we can rewrite the IDFT w.r.t. basis functions, and the connection between \mathbf{X} and \mathbf{H}^X can be expressed as follows:

$$\begin{aligned} \mathbf{X}[n] &= \frac{1}{T} \sum_{k=0}^{\frac{T}{2}} \left(\mathbf{a}_k \cos\left(\frac{2\pi kn}{T}\right) - \mathbf{b}_k \sin\left(\frac{2\pi kn}{T}\right) \right), \\ n &= 0, 1, \dots, T-1, \\ \mathbf{a}_k &= \begin{cases} \mathbf{H}_R[k], & k = 0, \frac{T}{2} \\ 2 \cdot \mathbf{H}_R[k], & k = 1, \dots, \frac{T}{2} - 1. \end{cases} \quad \mathbf{b}_k = \begin{cases} \mathbf{H}_I[k], & k = 0, \frac{T}{2} \\ 2 \cdot \mathbf{H}_I[k], & k = 1, \dots, \frac{T}{2} - 1. \end{cases} \end{aligned} \quad (2)$$

$\mathbf{H}_R[k]$ and $\mathbf{H}_I[k]$ represent the real and imaginary parts of $\mathbf{H}[k]$ respectively, where k refers to the frequency level, and $\mathbf{H}[k] = \mathbf{H}_R[k] + i\mathbf{H}_I[k]$. Eq. (2) provides an essential insight that the real and imaginary parts of the frequency spectrum can be interpreted as the coefficients of the cosine and sine basis functions, respectively. Thus, computing the frequency spectrum of the output time series is equivalent to computing the coefficients of cosine and sine basis functions, a process that aligns with the design of the N-BEATS [20] seasonal block.

Consequently, we highlight two issues in existing Fourier-based studies: inconsistent starting cycles and inconsistent series length issues. The inconsistent starting cycle issue arises because the real and imaginary parts only carry explicit meaning when combined and mixed with their corresponding basis functions. This is because combining a sine and cosine wave of the same frequency results in a phase-shifted cosine wave at that frequency with a modified amplitude, as shown below:

$$\begin{aligned} \mathbf{Z}(t) &= A \cos(\omega t) + B \sin(\omega t) = R \cos(\omega t - \phi), \\ R &= \sqrt{A^2 + B^2}, \quad \phi = \arctan(B, A). \end{aligned} \quad (3)$$

Therefore, the key information is embedded in the amplitude and arctangent of the real and imaginary values rather than the values themselves. The inconsistent series length issue occurs because the definition of frequency in hertz (Hz) depends on the length of the series. We present two cases, Cases I and II, to illustrate them in Figure 2, using a manually generated time series composed of sine and cosine basis functions, under the assumption that time series \mathbf{X} is used to forecast time series \mathbf{Y} .

In Case I, \mathbf{X} and \mathbf{Y} have the same frequency and series length but different starting cycles. When the real and imaginary components of the input frequency spectrum are processed independently to compute the output spectrum, no mathematical solution exists to establish such a mapping. However, their relationships can be easily identified through the amplitude and arctangent of the real and imaginary values, which are embedded within basis functions. As shown in Figure 2, a mathematical solution exists which is achievable through Eq. (2).

In Case II, \mathbf{X} and \mathbf{Y} have the same frequency and starting cycles but different series lengths. Although the frequency spectrum landscapes appear similar, their components (in Hz) carry different meanings. For example, an 8 Hz cosine

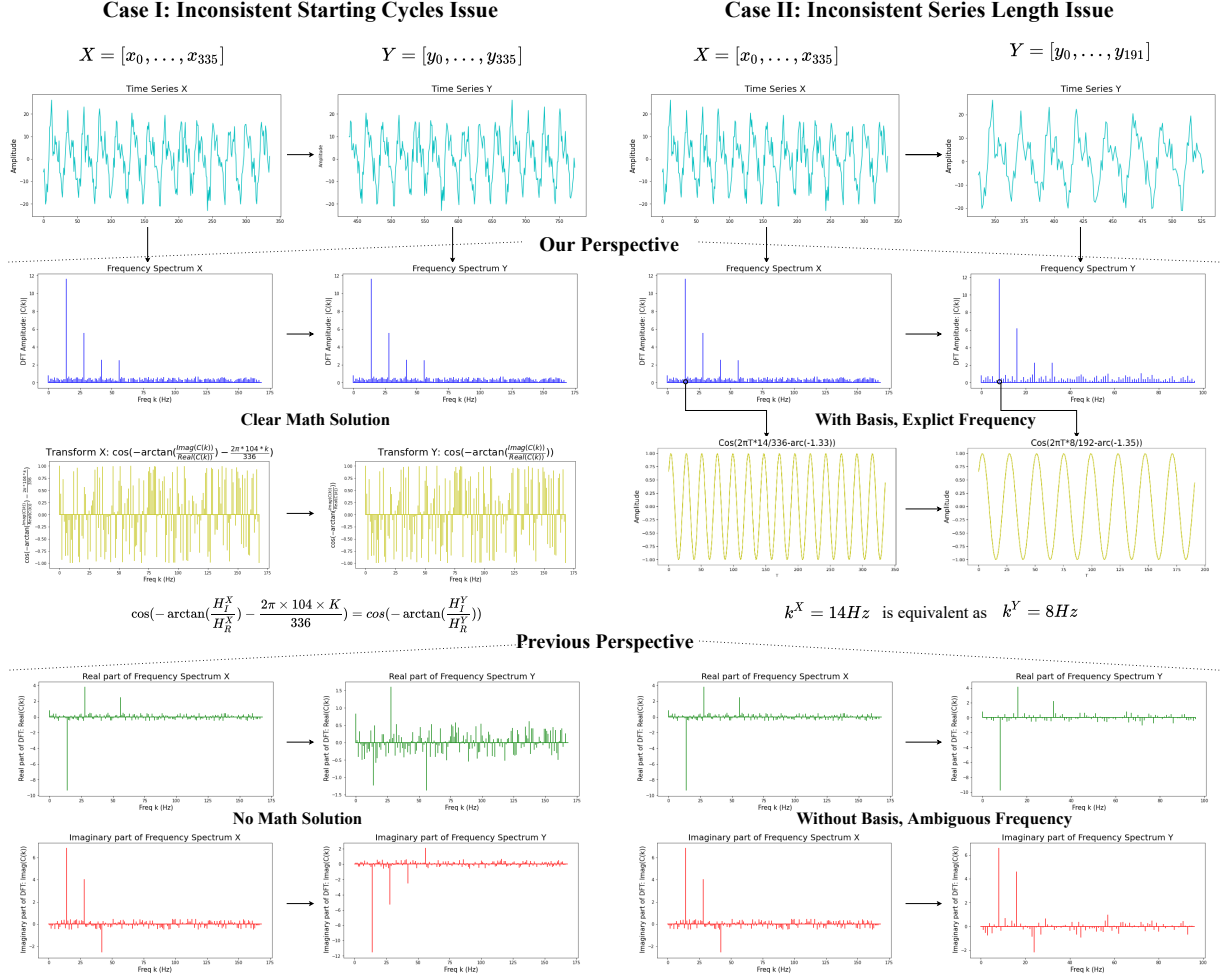


Fig. 2: Two Issues of Existing Fourier-based TSF Models: Inconsistent Starting Cycles Issue and Inconsistent Series Length Issue. In Case I, X and Y have a starting cycle gap of 104 over 336. In Case II, X and Y have different series lengths of 336 and 192, respectively.

function with a series length of 192 is equivalent to a 14 Hz cosine function with a series length of 336. Unfortunately, current models do not account for this frequency relationship precisely. As a result, the model faces challenges in precisely interpreting frequency components when series lengths vary. The presence of time-dependent basis functions makes it even harder. Instead, these issues can be easily resolved by incorporating basis functions, as including temporal information helps address them effectively.

IV. FBM: FOURIER BASIS MAPPING

A. Time-Frequency Features

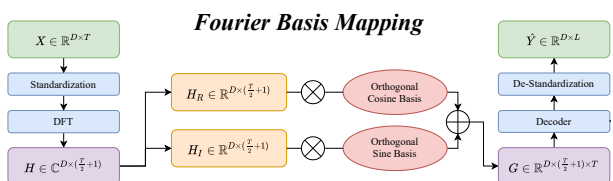


Fig. 3: Architecture of Fourier Basis Mapping Network.

To address two aforementioned issues, we introduce the Fourier basis mapping (FBM). The general architecture is shown in Figure 3. The primary strength of FBM lies in constructing time-frequency features, which capture explicit frequency information while preserving temporal characteristics. Subsequently, the downstream mapping considers the time-frequency space rather than solely the time or frequency space for forecasting. Since the basis functions incorporate information from the time domain, the mapping issue mentioned previously in the frequency domain no longer exists. To obtain the time frequency features, we multiply the real part of \mathbf{H} (denoted as \mathbf{H}_R) with the orthogonal cosine basis \mathbf{C} and the imaginary part of \mathbf{H} (denoted as \mathbf{H}_I) with the orthogonal sine basis \mathbf{S} , then add them together. This process is like breaking the time series into different frequency levels and also considering the phase shifts at each one. Let $\mathbf{N} = [0, 1, \dots, T-1]$, then \mathbf{C} and \mathbf{S} can be expressed as follows:

$$\mathbf{C} = \frac{1}{T} [1, 2 \cos(\frac{2\pi \mathbf{N}}{T}), \dots, 2 \cos(\frac{(T-1)\pi \mathbf{N}}{T}), \cos(\pi \mathbf{N})],$$

$$\mathbf{S} = -\frac{1}{T} [0, 2 \sin(\frac{2\pi \mathbf{N}}{T}), \dots, 2 \sin(\frac{(T-1)\pi \mathbf{N}}{T}), \sin(\pi \mathbf{N})]. \quad (4)$$

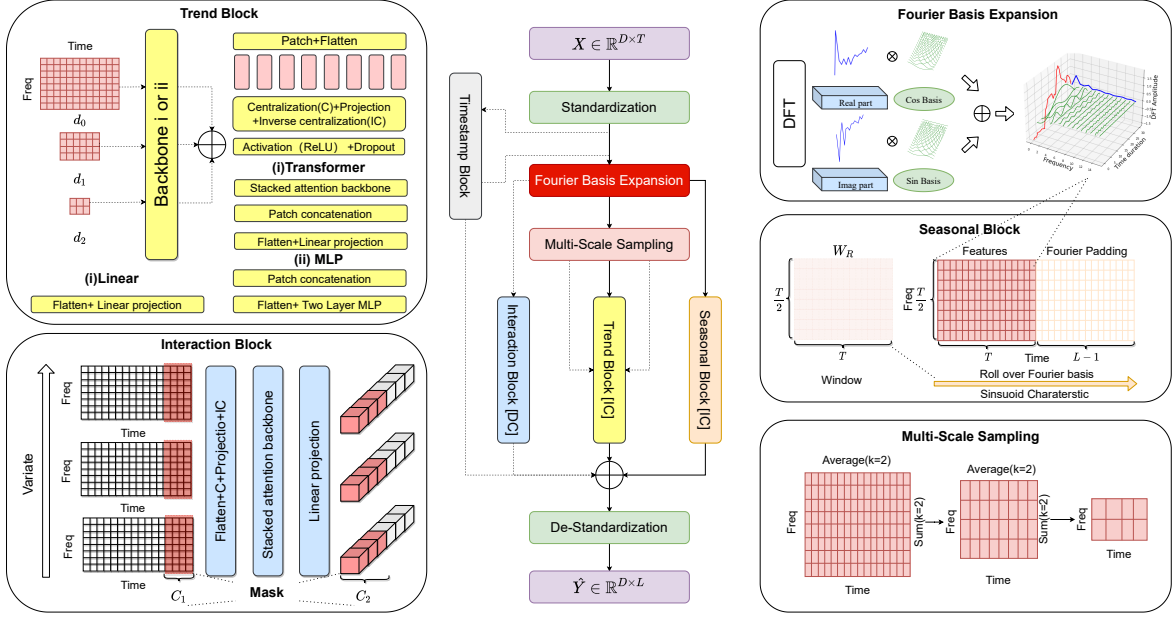


Fig. 4: FBM-S: A Three-Block Architecture for Trend, Seasonality, and Interaction. In the seasonal block, a rolling window is applied to the extended Fourier basis to extract seasonal patterns. In the trend block, we allow the use of linear, MLP-based, or Transformer-based architectures. In addition, we introduce techniques such as patching based on time segments of the time-frequency features, centralization and inverse centralization before and after the initial projection, and multi-scale down-sampling using both average and sum kernels. In the interaction block, a masking mechanism is developed to model the relationship between the masked input sequence length C_1 and the masked output sequence length C_2 , as interaction effects typically occur over short periods. Centralization technique is also applied in the interaction block to improve the robustness of the extracted features. ID refers to independent channel modeling, while DC refers to dependent channel modeling.

B. The Plug-and-Play Effects for FBM-L, FBM-NL, FBM-NP

Since our time-frequency features preserve time-domain information, they can be applied to any method by simply adjusting the initial projection layer to map the time-frequency features into the hidden state. This projection considers both time and frequency modalities, which leads to improved performance. We first design three decoders to demonstrate the effectiveness of time-frequency features by plugging them into existing mapping methods for better performance: linear (L), non-linear three-layer perception (NL) and non-linear (NP). Consequently, three FBM variants are generated: FBM-L with linear network, FBM-NL with MLP network, and FBM-NP with Transformer-based network with patching. The first variant consists of a single vanilla linear layer and serves as a plug-and-play version of NLinear [48]. While NLinear maps input time series features to output time series using a single layer, our approach maps time-frequency features to output time series using also a single layer. The second variant includes three fully connected layers with ReLU activation functions, representing a deeper version of NLinear. NLinear [48] has shown that increasing the depth of a network by stacking MLP layers can lead to degraded performance. However, we prove that increasing the network depth tends to improve results when using time-frequency features. Thus, even a very simple one-layer or three-layer neural network can achieve strong performance by mapping in the time-

frequency space. The last variant serves as a plug-and-play version of PatchTST [24], with the only difference lying in the initial projection. Specifically, PatchTST performs patching based on time segments and projects the patched features into the hidden space. Similarly, we perform patching based on time segments of the time-frequency features, then flatten the patches and apply a projection. We also show that FBM-NP can outperform PatchTST with fewer patches and improved efficiency by effectively utilizing time-frequency features.

C. FBM-S: A Synergetic Architecture

We propose a more efficient and effective approach for modeling time-frequency features: a synergetic FBM model, namely FBM-S, which captures trend, seasonality, and interaction effects through three distinct blocks. We consider different architectures for time-frequency features to study those effects, respectively. In Figure 4, we provide the overall architecture. Since we perform standardization at the beginning, we remove the first frequency level, as it is always zero. The timestamp block is directly copied from [53] and is used only for hourly Long-term TSF datasets.

Seasonal Block: In the seasonal block, the output features are expected to reflect seasonal characteristics. Therefore, using a rolling window filter is an optimal way to capture these patterns. This is because all the basis functions exhibit sinusoidal characteristics. Therefore, after generating the time-frequency features, we apply the Fourier padding to extend the

Fourier basis with an additional length of $L-1$. We then apply a rolling window with weights $\mathbf{W} \in \mathbb{R}^{T \times \frac{T}{2}}$ over the padded features to extract the seasonal components. The $\hat{\mathbf{Y}}_S$ refers to the output of the seasonal block, and the mathematical formula can be shown as follows:

$$\begin{aligned} \hat{\mathbf{Y}}_S[v] &= \frac{2}{T} \sum_{n=0}^{T-1} \sum_{k=1}^{\frac{T}{2}} \left(\mathbf{a}_k \left(\mathbf{W}_{n,k} \cdot \cos \left(\frac{2\pi k(n+v)}{T} \right) \right) \right. \\ &\quad \left. + \frac{2}{T} \sum_{n=0}^{T-1} \sum_{k=1}^{\frac{T}{2}} \left(\mathbf{b}_k \left(\mathbf{W}_{n,k} \cdot \sin \left(-\frac{2\pi k(n+v)}{T} \right) \right) \right), \right. \\ &\quad \left. v = 0, 1, \dots, L-1, \right. \\ \mathbf{a}_k &= \begin{cases} \frac{1}{2} \cdot \mathbf{H}_R[k], & k = 0, \frac{T}{2}, \\ \mathbf{H}_R[k], & k = 1, \dots, \frac{T}{2} - 1. \end{cases} \end{aligned} \quad (5)$$

Here, we apply a small trick: we first let the weights multiply the padded Fourier basis functions, and then multiply the result with the real and imaginary values. This significantly improves both memory efficiency and backpropagation speed instead of using the default convolution in PyTorch.

Interaction Block with Masking: We consider channel interactions within the interaction block, which is particularly important in short-term TSF, since interactions usually occur over short periods. For example, a traffic overload usually affects only nearby regions for a brief period; in the long run, the time series is primarily governed by its own trend and seasonal effects. Inspired by this observation, we utilize only the most recent time-frequency features for modeling, using the red-highlighted mask shown in Figure 4, which corresponds to an input mask of length C_1 . In addition, we also find that its influence does not last for a long period. Therefore, we use an additional output mask C_2 for long-term TSF. We also introduce centralization for segments of time-frequency features to improve the robustness of the extracted hidden representations, as it helps the model better understand whether a time series is in a normal, peak, or off-peak stage, which is crucial for interaction modeling. The experimental results show that this interaction backbone significantly improves both short-term and long-term TSF performance.

Trend Block: We aim to capture non-linear trending effects, but we also retain the simple linear architecture as an option. To this end, we adopt either an MLP-based architecture with patching or a Transformer-based architecture with patching. This block integrates the strengths of FBM-L, FBM-NP, and FBM-NL. The PatchTST model has demonstrated that patching is an effective technique for time-domain modeling. Building upon this, we further show that patching is also beneficial for time-frequency features. In FBM-NP, we find that patching time-frequency features based on time segment is particularly beneficial for Transformer models, and thus we also apply this strategy to the MLP-based network. In the previous FBM-NL method, we used whole flattened time-frequency features as initial input, which increased the burden of initial projection. However, when patching is applied, the complexity of the initial projection layer can be reduced by a factor of P^2 , where P is the number of patches. It reduces the modeling complexity while also achieving better performance.

Thus, after patching, we perform the projection of the patched time-frequency features. Since we want to capture the trend effects here, we apply a non-linear activation function after the initial projection. This is always effective; even though the downstream backbones are nonlinear, adding the activation function in the initial projection increases the robustness of the extracted features. Finally, we summarize the only difference between the MLP-based network and the Transformer-based network is that the MLP-based version removes the stack of attention layers and replaces it with a single projection layer with activation, as the final projection is always the same format. The results in Section V show that the MLP-based method consistently achieves better efficiency and performance, indicating that we can use a simpler downstream architecture with time-frequency features. Additionally, we introduce centralization and multi-scale down-sampling in the trend block to further enhance performance.

Centralization: Implementing centralization and inverse centralization techniques proves to be highly effective throughout the modeling process. This strategy enhances performance not only at the initial and final stages, but also during intermediate phases, particularly before and after projecting patched time-frequency features within both the trend and interaction blocks. Although entire time-frequency features exhibit a zero mean due to the initial standardization, the mean of the flattened features within each patch deviates from zero. Consequently, applying centralization prior to projection and decentralization afterward normalizes their distributions, thereby improving model performance. In notation $x_{dpn}^{(i)}$, $d \in [1, \dots, D]$ denotes variate index, $p \in [1, \dots, P]$ indicates the patch index, and $n \in [1, \dots, N]$ denotes the elements within the patched time-frequency features, and i refers to the i -th layer. Specifically, $N = \frac{T^2}{2P}$ in the trend block, whereas in the seasonal block, $N = C_1 \times \frac{T}{2}$ as only the last patch with mask C_1 will be involved in the modeling. The corresponding mathematical formulas are shown below:

$$\begin{aligned} \mathbb{E}_t \left[x_{dp}^{(i)} \right] &= \frac{1}{N} \sum_{n=1}^N x_{dpn}^{(i)}, \\ \text{Var} \left[x_{dp}^{(i)} \right] &= \frac{1}{N} \sum_{n=1}^N \left(x_{dpn}^{(i)} - \mathbb{E}_t \left[x_{dp}^{(i)} \right] \right)^2, \\ x_{dpn}^{(i)} &= \gamma_d \left(\frac{x_{dpn}^{(i)} - \mathbb{E}_t \left[x_{dp}^{(i)} \right]}{\sqrt{\text{Var} \left[x_{dp}^{(i)} \right] + \epsilon}} \right) + \beta_d, \\ x_{dpn}^{(j)} &= \sqrt{\text{Var} \left[x_{dp}^{(i)} \right] + \epsilon} \cdot \left(\frac{x_{dpn}^{(j)} - \beta_d}{\gamma_d} \right) + \mathbb{E}_t \left[x_{dp}^{(i)} \right]. \end{aligned} \quad (6)$$

where i and j is the initial and final layer within the trend and interaction blocks and $\gamma, \beta \in \mathbb{R}^D$ are learnable affine parameter vectors. Standardization refers to the case when the affine transformation is not applied.

Multi-scale Down-sampling: We also introduce a multi-scale mapping mechanism, inspired by the TimeMixer [17] and U-Net [55] architectures. Specifically, we downsample the time-frequency features to generate lower-resolution represen-

tations by averaging along the time dimension and summing across the frequency dimension, resulting in downsampled features d_1 and d_2 with kernel sizes of two and four, respectively. This approach is particularly effective for handling high-granularity data, such as PEMS with five-minute intervals. The multi-scale features are processed through separate layers and aggregated subsequently.

V. PRELIMINARY EXPERIMENTAL SETUP

A. Data

We conduct our experiments on twelve real-world datasets: ETT¹ (ETTh1, ETTh2, ETTm1, ETTm2), Electricity (ECL)², Traffic (TRA)³, Weather (WTH)⁴, Exchange rate (Exchange)⁵ and PEMS⁶ (PEMS04, PEMS08M, PEMS03, PEMS07) and M4⁷ (yearly, quarterly, monthly, weekly, daily and hourly). The granularity of ETTh1, ETTh2, Electricity, and Traffic is at an hourly time scale; the granularity of ETTm1 and ETTm2 is at a fifteen-minute time scale; the granularity of Weather is at a ten-minute time scale; the granularity of Exchange is at a daily time scale; and the granularity of PEMS is at a five-minute time scale. In M4 dataset, participants are tasked with forecasting a fixed number of time steps: 6 for yearly series, 8 for quarterly, 18 for monthly, 13 for weekly, 14 for daily and 48 for hourly series, respectively. The ETT datasets include seven oil and load characteristics of electricity transformers, which span from July 2016 to July 2018. Traffic comprises hourly road occupancy rates measured by 862 sensors in the San Francisco Bay area from 2015 to 2016. Electricity records the hourly electricity consumption (in kWh) of 321 clients from 2012 to 2014. Weather includes 21 weather indicators for 2020 in Germany, such as air temperature, humidity, and so on. Exchange tracks the daily exchange rates of eight countries from 1990 to 2016. PEMS contains the public traffic network data in California with four public subsets. The M4 dataset was created by selecting a random sample of 100,000 time series from the ForeDeCk database.

B. Baselines

We compare FBM with eight baseline methods: NLinear, PatchTST, iTransformer, TimeMixer, N-BEATS, CrossGNN, FITS and FreTS on eight datasets for Long-term TSF(LTSF). Furthermore, we compare FBM with six baseline methods: the NLinear, PatchTST, TimeMixer, iTransformer, FiLM, and TimesNet on four PEMS datasets for short-term TSF(STSF). These methods are chosen because they represent six categories of modeling methods: (1) Linear method: NLinear [48]; (2) Transformer-based methods: iTransformer [35] and PatchTST [24]; (3) MLP-based methods: N-BEATS [20], FreTS [22], and TimeMixer [17]; (4) RNNs-based method: FiLM; (5) CNNs-based method: TimesNet [16]; and (4)

Fourier-based methods: N-BEATS [20], FITS [49], FreTS [22], CrossGNN [40], FiLM [9] and TimesNet [16].

C. Experiment Settings

The mean squared error (MSE) and mean absolute error (MAE) are used as evaluation metrics for both LTSF and STSF. The look-back window is set to 336, and the forecast horizons are set to 96, 192, 336, 720 for LTSF and 12, 24, 48, 96 for STSF. We split the ETT dataset into 12/4/4 months and all the other datasets into training, validation, and test sets by the ratio of 6.5/1.5/2. We use the same batch size for all baseline methods to ensure fair comparisons, where 128 for ETTh1, ETTm1, ETTh2, ETTm2, WTH, and Exchange, 64 for PEMS03, PEMS04, PEMS07, and PEMS08, and 16 for Electricity and Traffic. On the other hand, the experimental setup for the M4 dataset follows that of TimeMixer [17] as well as the selected baseline methods. The input length of M4 is twice the forecast horizon. The hyperparameters are shown in Table I, and the model structure of FBM-S and the meaning of those hyperparameters are elaborated in Section VI-D. For more implementation details, please refer to our project page. **We use the same random seed and provide all implementation details and scripts on the project page to ensure the reproducibility of the reported experiments.**

TABLE I: Hyperparameter Details for Different Dataset.

	Trend	Seasonal	Interaction	Patch	Multi-Scale	P	h_1	h_2	h_3	K	C_1	C_2	Timestamp
PEMS03	MLP	✓	✓	✓	d_1	14	256	1440	512	3	24	L	✓
PEMS04	MLP	✓	✓	✓	d_1	14	256	1440	512	3	24	L	✓
PEMS07	MLP	✓	✓	✓	d_1	14	256	1440	512	3	24	L	✓
PEMS08	MLP	✓	✓	✓	d_1	14	256	1440	512	3	24	L	✓
ECL	MLP	✓	✓	✓	d_0	14	256	1440	512	3	24	24	✓
Traffic	Transformer	✓	✓	✓	d_0	14	128	128	512	4	T	L	✓
WTH	MLP	✓	✓	✓	$d_0 + d_1$	14	256	1440	256	3	96	12	✓
ETTh1	MLP	✓	✓	✓	$d_0 + d_1 + d_2$	14	128	1440	128	3	48	48	✓
ETTh2	MLP	✓	✓	✓	d_0	14	128	1440	128	3	48	48	✓
ETTh1	Linear	✓	✓	✓	d_0	-	-	-	-	-	-	-	✓
ETTh2	Linear	✓	✓	✓	d_0	-	-	-	-	-	-	-	✓
Exchange	Linear	✓	✓	✓	d_0	-	-	-	-	-	-	-	✓
M4	MLP	✓	✓	✓	d_0	-	1440	1440	-	-	-	-	✓

VI. EXPERIMENT RESULTS

A. Overview

We evaluate the forecasting performance of four FBM variants against diverse baseline models for both Long-term TSF (LTSF) and short-term TSF (STSF). These baselines cover a wide range of architectures, including time- and frequency-based mapping methods. Table II presents results for LTSF, while Table III and Table IV display results for STSF. In our experiments, we first demonstrate the effectiveness of time-frequency features by proposing three FBM variants: FBM-L, FBM-NL, and FBM-NP, which can serve as plug-and-play modules within existing methods. We then demonstrate that our time-frequency learning framework, implemented via the FBM-S model, has the potential to achieve state-of-the-art performance across nearly all datasets for both LTSF and STSF, as detailed in Sections VI-B and VI-C. Notably, we perform an efficiency analysis and elaborate on the model structure, including the seasonal, trend, and interaction blocks, in Section VI-D. The effectiveness of each technique for time-frequency features is thoroughly validated through ablation studies in Section VI-E. We provide visualizations to help understand the effects of rolling windows in Section VI-F, and a case study in Section VI-G. Finally, we provide guidelines for architecture design from the perspective of frequency spectrum distribution in Section VI-H.

¹<https://github.com/zhouhaoyi/ETDataset>

²<https://archive.ics.uci.edu/ml/datasets/ElectricityLoadDiagrams20112014>

³<http://pems.dot.ca.gov>

⁴<https://www.bgc-jena.mpg.de/wetter/>

⁵<https://github.com/laiguokun/multivariate-time-series-data>

⁶<https://www.kaggle.com/datasets/elmahy/pems-dataset>

⁷<https://paperswithcode.com/dataset/m4>

TABLE II: Performance of FBM-S, FBM-L, FBM-NL, and FBM-NP Compared to Eight Baseline Methods on Eight Datasets for Long-term TSF.

Method	FBM-S				FBM-L				FBM-NL				FBM-NP				NLinear [48]		PatchTST [24]		iTransformer [35]		TimeMixer [17]		N-BEATS [20]		CrossGNN [40]		FITS [49]		FreTS [22]	
Error	MSE	MAE	MSE	MAE	MSE	MAE	MSE	MAE	MSE	MAE	MSE	MAE	MSE	MAE	MSE	MAE	MSE	MAE	MSE	MAE	MSE	MAE	MSE	MAE	MSE	MAE	MSE	MAE	MSE	MAE		
ETTh1	96	0.363	0.389	0.366	0.390	0.368	0.395	0.367	0.395	0.391	0.416	0.374	0.399	0.399	0.417	0.385	0.408	0.387	0.410	0.376	0.400	0.368	0.392	0.404	0.423							
	192	0.399	0.409	0.403	0.411	0.408	0.418	0.407	0.416	0.421	0.426	0.417	0.422	0.436	0.440	0.429	0.432	0.428	0.434	0.419	0.427	0.404	0.412	0.461	0.460							
	336	0.402	0.413	0.418	0.420	0.425	0.430	0.433	0.438	0.435	0.435	0.431	0.436	0.446	0.451	0.456	0.450	0.448	0.447	0.439	0.442	0.419	0.435	0.488	0.480							
	720	0.403	0.433	0.414	0.438	0.456	0.466	0.439	0.459	0.443	0.457	0.445	0.463	0.502	0.503	0.457	0.462	0.466	0.471	0.447	0.465	0.431	0.458	0.566	0.553							
ETTh2	96	0.271	0.331	0.271	0.331	0.287	0.343	0.280	0.340	0.283	0.342	0.276	0.338	0.303	0.362	0.276	0.339	0.303	0.363	0.283	0.344	0.276	0.338	0.327	0.388							
	192	0.332	0.373	0.332	0.373	0.351	0.386	0.342	0.382	0.350	0.387	0.341	0.378	0.372	0.403	0.340	0.381	0.364	0.402	0.342	0.387	0.336	0.377	0.428	0.450							
	336	0.320	0.376	0.321	0.376	0.352	0.394	0.354	0.401	0.344	0.395	0.332	0.385	0.401	0.424	0.362	0.404	0.360	0.407	0.361	0.408	0.324	0.379	0.499	0.497							
	720	0.361	0.408	0.369	0.412	0.397	0.432	0.386	0.424	0.395	0.436	0.379	0.420	0.420	0.446	0.398	0.433	0.428	0.465	0.423	0.460	0.465	0.373	0.416	0.727	0.637						
ETTm1	96	0.278	0.332	0.301	0.343	0.286	0.339	0.293	0.346	0.307	0.349	0.295	0.344	0.309	0.361	0.303	0.350	0.324	0.367	0.300	0.343	0.305	0.347	0.326	0.373							
	192	0.317	0.358	0.337	0.364	0.324	0.365	0.334	0.368	0.347	0.374	0.333	0.370	0.345	0.383	0.356	0.385	0.363	0.388	0.335	0.369	0.338	0.366	0.359	0.392							
	336	0.356	0.382	0.371	0.384	0.359	0.385	0.371	0.389	0.377	0.390	0.363	0.394	0.380	0.401	0.366	0.392	0.400	0.408	0.375	0.390	0.372	0.386	0.389	0.408							
	720	0.412	0.418	0.425	0.415	0.422	0.424	0.426	0.420	0.436	0.425	0.421	0.420	0.448	0.442	0.435	0.434	0.468	0.448	0.429	0.420	0.427	0.416	0.445	0.441							
ETTm2	96	0.164	0.252	0.164	0.252	0.165	0.254	0.167	0.258	0.169	0.259	0.173	0.261	0.180	0.272	0.174	0.258	0.168	0.259	0.164	0.252	0.167	0.256	0.202	0.288							
	192	0.219	0.290	0.219	0.290	0.225	0.296	0.224	0.296	0.223	0.294	0.255	0.306	0.239	0.311	0.238	0.300	0.225	0.301	0.220	0.294	0.222	0.293	0.250	0.322							
	336	0.273	0.326	0.271	0.325	0.276	0.331	0.277	0.331	0.277	0.331	0.285	0.336	0.389	0.341	0.272	0.327	0.282	0.336	0.276	0.330	0.277	0.329	0.328	0.368							
	720	0.365	0.382	0.364	0.381	0.365	0.386	0.367	0.386	0.371	0.387	0.365	0.386	0.374	0.392	0.368	0.389	0.376	0.394	0.372	0.390	0.366	0.382	0.431	0.436							
Electricity	96	0.127	0.220	0.142	0.237	0.132	0.227	0.133	0.227	0.143	0.239	0.133	0.227	0.137	0.232	0.134	0.230	0.144	0.240	0.147	0.246	0.145	0.242	0.145	0.245							
	192	0.144	0.237	0.155	0.248	0.149	0.243	0.149	0.242	0.157	0.250	0.151	0.244	0.156	0.249	0.153	0.245	0.158	0.252	0.161	0.258	0.158	0.253	0.158	0.255							
	336	0.161	0.254	0.172	0.265	0.167	0.261	0.167	0.261	0.174	0.267	0.167	0.261	0.171	0.266	0.172	0.267	0.175	0.269	0.178	0.274	0.174	0.269	0.178	0.275							
	720	0.195	0.285	0.212	0.297	0.207	0.295	0.208	0.295	0.214	0.299	0.210	0.297	0.195	0.288	0.212	0.298	0.217	0.304	0.214	0.299	0.213	0.301	0.220	0.315							
Traffic	96	0.357	0.246	0.421	0.281	0.384	0.264	0.373	0.253	0.425	0.288	0.381	0.257	0.376	0.263	0.381	0.261	0.429	0.295	0.428	0.291	0.421	0.282	0.434	0.313							
	192	0.382	0.257	0.434	0.286	0.399	0.269	0.396	0.266	0.438	0.291	0.402	0.270	0.396	0.274	0.408	0.273	0.441	0.299	0.441	0.295	0.435	0.288	0.471	0.311							
	336	0.393	0.263	0.447	0.292	0.419	0.282	0.411	0.276	0.452	0.300	0.422	0.283	0.407	0.283	0.434	0.297	0.455	0.307	0.455	0.302	0.448	0.293	0.493	0.321							
	720	0.430	0.285	0.477	0.309	0.448	0.297	0.442	0.291	0.482	0.317	0.454	0.296	0.449	0.305	0.469	0.319	0.486	0.326	0.486	0.318	0.478	0.310	0.535	0.339							
Weather	96	0.147	0.196	0.159	0.207	0.152	0.199	0.156	0.204	0.176	0.226	0.156	0.206	0.162	0.211	0.158	0.204	0.186	0.238	0.163	0.227	0.149	0.198	0.159	0.218							
	192	0.189	0.238	0.203	0.247	0.194	0.242	0.198	0.245	0.220	0.262	0.200	0.246	0.204	0.249	0.197	0.246	0.227	0.275	0.205	0.261	0.196	0.244	0.207	0.270							
	336	0.238	0.276	0.252	0.285	0.244	0.282	0.248	0.285	0.265	0.296	0.252	0.285	0.248	0.285	0.242	0.281	0.274	0.307	0.250	0.295	0.245	0.283	0.252	0.299							
	720	0.311	0.328	0.319	0.335	0.317	0.334	0.319	0.337	0.332	0.345	0.321	0.336	0.322	0.335	0.319	0.335	0.342	0.361	0.320	0.347	0.321	0.338	0.319	0.342							
Exchange	96	0.093	0.211	0.093	0.211	0.104	0.226	0.096	0.196	0.098	0.219	0.104	0.227	0.128	0.254	0.119	0.247	0.147	0.274	0.093	0.211	0.109	0.235	0.209	0.350							
	192	0.194	0.308	0.195	0.309	0.210	0.326	0.196	0.312	0.203	0.316	0.210	0.325	0.241	0.353	0.238	0.354	0.312	0.406	0.188	0.305	0.229	0.350	0.346	0.437							
	336	0.346	0.419	0.347	0.421	0.398	0.460	0.353	0.425	0.356	0.426	0.366	0.435	0.393	0.459	0.417	0.472	0.522	0.532	0.363	0.430	0.400	0.463	0.634	0.583							
	720	0.963	0.732	0.965	0.732	1.040	0.762	0.970	0.734	0.965	0.733	1.026	0.757	1.00	0.763	1.074	0.790	1.412	0.907	0.931	0.722	1.095	0.781	2.418	1.233							
Average		0.309	0.332	0.323	0.339	0.325	0.344	0.321	0.340	0.333	0.349	0.326	0.344	0.341	0.353	0.335	0.352	0.366	0.371	0.330	0.350	0.331	0.347	0.431	0.406							

B. Long-term TSF Results

FBM-L vs Linear Network: The FBM-L model demonstrates superior performance over the NLinear model across all datasets and prediction horizons. Specifically, it reduces the average MSE from 0.333 to 0.323 and the MAE from 0.349 to 0.339. This enhancement underscores the effectiveness of FBM-L, which employs Fourier basis expansion to decompose temporal data based on frequency components. By operating in the time-frequency space, the model can better distinguish noise from meaningful effects, leading to improved forecast accuracy. The gains are particularly notable in datasets such as ETTh1 and ETTh2, which contain richer frequency components and higher levels of noise. Furthermore, our experiments reveal that even a simple vanilla linear network FBM-L has the potential to outperform SOTA DNN-based architectures.

FBM-NL vs MLP-based Methods and FBM-NP VS Transformer-based Methods: In [48], they report that increasing the depth of the network does not improve performance for time-based method. In contrast, FBM-NL demonstrates that increasing the depth of the network is beneficial for most datasets when time-frequency features are incorporated. This highlights the potential of the time-frequency learning framework. It considers both time and frequency characteristics in the initial projection. Additionally, FBM-NL performs better than TimeMixer and FBM-NP performs better than PatchTST at most of the time, where the for-

mer two are MLP-based networks, and the latter two are Transformer-based networks with patching. The experimental results further demonstrate the effectiveness of time-frequency features, suggesting that extracting time-frequency features efficiently is more advantageous than relying solely on deeper architectures. It is worth noting that TimeMixer also decomposes the original time series into trend and seasonal effects, but its performance largely depends on the choice of the moving average kernel size or Top-k frequencies. In contrast, our Fourier basis expansion automatically decomposes various effects hierarchically within distinct frequency levels. Although FBM-NP uses fewer patches than PatchTST, it even achieves better performance. Our FBM variants also consistently outperform other Transformer-based and MLP-based architectures, including iTransformer and N-BEATS and so on.

FBM Variants vs. Fourier-based Methods: We also observe that FBM variants make a significant improvement over all Fourier-based methods, including N-BEATS, FreTS, CrossGNN, and FITS. This discrepancy may largely be attributed to the inconsistent starting cycles and series length issues discussed in Section III. Notably, FITS and CrossGNN also emphasize the importance of the amplitude of real and imaginary values. However, they overlook the fact that Fourier basis functions are time-dependent when the input length is not divisible by a certain frequency level. Consequently,

TABLE III: Performance of FBM-S, FBM-L, FBM-NL, and FBM-NP Compared to Six Baseline Methods on PEMS Datasets for Short-term TSF.

Method		FBM-S		FBM-L		FBM-NL		FBM-NP		NLinear [48]		PatchTST [24]		TimeMixer [17]		iTransformer [35]		FiLM [9]		TimesNet [16]	
Error		MSE	MAE	MSE	MAE	MSE	MAE	MSE	MAE	MSE	MAE	MSE	MAE	MSE	MAE	MSE	MAE	MAPE	MAE	MSE	MAE
PEMS03	12	0.057	0.156	0.077	0.183	<u>0.060</u>	<u>0.161</u>	0.061	0.162	0.078	0.184	0.065	0.174	0.062	0.164	0.061	0.163	0.108	0.223	0.089	0.199
	24	0.069	0.170	0.111	0.210	<u>0.071</u>	<u>0.171</u>	0.073	0.174	0.114	0.214	0.075	0.179	0.074	0.182	0.080	0.189	0.179	0.274	0.096	0.204
	48	0.085	0.188	0.159	0.243	0.094	<u>0.194</u>	0.101	0.201	0.162	0.248	0.101	0.208	<u>0.092</u>	0.201	0.103	0.213	0.235	0.321	0.115	0.220
	96	0.103	0.206	0.195	0.267	0.118	<u>0.215</u>	0.126	0.222	0.198	0.273	0.139	0.240	<u>0.105</u>	0.216	0.123	0.229	0.201	0.299	0.118	0.229
PEMS04	12	0.062	0.157	0.088	0.195	<u>0.071</u>	0.172	0.071	<u>0.170</u>	0.089	0.196	0.075	0.179	0.071	0.173	0.073	0.176	0.118	0.237	0.091	0.196
	24	0.072	0.168	0.120	0.223	0.080	0.179	0.084	0.182	0.123	0.228	0.085	0.190	<u>0.073</u>	<u>0.174</u>	0.086	0.189	0.177	0.278	0.090	0.190
	48	0.088	0.182	0.167	0.257	0.099	0.194	0.107	0.204	0.171	0.265	0.108	0.211	<u>0.089</u>	<u>0.189</u>	0.107	0.209	0.241	0.325	0.094	0.193
	96	0.104	0.196	0.207	0.282	0.125	0.216	0.135	0.224	0.210	0.287	0.130	0.229	<u>0.107</u>	<u>0.211</u>	0.127	0.227	0.207	0.295	0.112	0.215
PEMS07	12	0.049	0.137	0.073	0.180	0.053	<u>0.148</u>	0.054	0.150	0.073	0.180	0.057	0.164	0.053	0.151	<u>0.053</u>	<u>0.148</u>	0.101	0.221	0.079	0.182
	24	0.056	0.145	0.107	0.212	0.063	0.160	0.062	0.157	0.109	0.216	0.065	0.172	<u>0.061</u>	<u>0.158</u>	0.069	0.171	0.199	0.299	0.080	0.177
	48	0.064	0.155	0.157	0.251	0.074	<u>0.168</u>	0.079	0.175	0.160	0.255	0.079	0.189	<u>0.072</u>	0.172	0.077	0.177	0.238	0.331	0.084	0.183
	96	0.072	0.162	0.197	0.279	0.090	<u>0.184</u>	0.093	0.186	0.200	0.285	0.093	0.199	0.091	0.199	<u>0.087</u>	0.190	0.190	0.281	0.089	0.188
PEMS08	12	0.055	0.147	0.081	0.189	<u>0.060</u>	<u>0.159</u>	0.061	0.159	0.081	0.190	0.062	0.165	0.060	0.160	0.062	0.165	0.108	0.226	0.094	0.204
	24	0.064	0.157	0.115	0.211	0.069	0.165	0.069	0.168	0.118	0.227	0.072	0.178	0.068	0.170	<u>0.066</u>	<u>0.160</u>	0.182	0.285	0.097	0.198
	48	0.073	0.167	0.173	0.264	0.084	<u>0.179</u>	0.085	0.183	0.180	0.271	0.088	0.196	<u>0.080</u>	0.183	0.090	0.195	0.261	0.341	0.102	0.204
	96	0.083	0.177	0.228	0.298	0.102	0.195	0.103	0.196	0.234	0.303	0.105	0.207	0.098	0.201	<u>0.091</u>	<u>0.183</u>	0.233	0.302	0.121	0.226
Average		0.072	0.166	0.140	0.234	0.082	<u>0.178</u>	0.085	0.182	0.143	0.238	0.087	0.192	<u>0.078</u>	0.181	0.084	0.186	0.186	0.283	0.096	0.200

TABLE IV: Performance of FBM-S Compared to Thirteen Baseline Methods on the M4 Dataset for Univariate TSF. The sampling frequencies and forecast horizons ranging from 6 to 48. A lower SMAPE, MASE or OWA indicates a better prediction.

Models		FBM-S	TimeMixer [17]	TimesNet [16]	N-HITS [21]	N-BEATS [20]	SCINet [12]	PatchTST [24]	MICN [13]	FiLM [9]	LightTS [56]	DLinear [48]	FEDformer [39]	Stationary [57]	Autoformer [27]
Yearly	SMAPE	13.199	13.206	13.387	13.418	13.436	18.605	16.463	25.022	17.431	14.247	16.965	13.728	13.717	13.974
	MASE	2.953	2.916	2.996	3.045	3.043	4.471	3.967	7.162	4.043	3.109	4.283	3.048	3.078	3.134
	OWA	0.775	0.776	0.786	0.793	0.794	1.132	1.003	1.667	1.042	0.827	1.058	0.803	0.807	0.822
Quarterly	SMAPE	9.955	9.996	10.100	10.202	10.124	14.871	10.644	15.214	12.925	11.364	12.145	10.792	10.958	11.338
	MASE	1.163	1.166	1.182	1.194	1.169	2.054	1.278	1.963	1.664	1.328	1.520	1.283	1.325	1.365
	OWA	0.876	0.825	0.890	0.899	0.886	1.424	0.949	1.407	1.193	1.000	1.106	0.958	0.981	1.012
Monthly	SMAPE	12.318	12.605	12.670	12.791	12.677	14.925	13.399	16.943	15.407	14.014	13.514	14.260	13.917	13.958
	MASE	0.903	0.919	0.933	0.969	0.937	1.131	1.031	1.442	1.298	1.053	1.037	1.102	1.097	1.103
	OWA	0.852	0.869	0.878	0.899	0.880	1.027	0.949	1.265	1.144	0.981	0.956	1.012	0.998	1.002
Others	SMAPE	4.358	4.564	4.891	5.061	4.925	16.655	6.558	41.985	7.134	15.880	6.709	4.954	6.302	5.485
	MASE	3.041	3.115	3.302	3.391	3.216	15.034	4.511	62.734	5.09	11.434	4.953	3.264	4.064	3.865
	OWA	0.938	0.982	1.035	1.040	1.053	4.123	1.401	14.313	1.553	3.474	1.487	1.036	1.304	1.187
Average	SMAPE	11.555	11.723	11.829	11.927	11.851	15.542	13.152	19.638	14.863	13.525	13.639	12.840	12.780	12.909
	MASE	1.544	1.559	1.585	1.613	1.559	2.831	1.945	5.947	2.207	2.111	2.095	1.701	1.756	1.771
	OWA	0.830	0.840	0.851	0.861	0.855	1.309	0.998	2.279	1.125	1.051	1.051	0.918	0.930	0.959

Some results in this table are directly copied from TimeMixer (2024), as we use the same evaluation method and setting they used.

mapping in the frequency domain disregards time-domain characteristics and fails to capture fine-grained relationships. For instance, CrossGNN retains only the value from the first cycle but fails to capture variations in subsequent cycles or shifts in their phases across different frequency levels. In contrast, FBM variants offer a more effective representation of time-frequency features by performing the mapping within the time-frequency space.

FBM-S vs. the Other Three FBM Variants: We decompose the separated effects into trend, seasonal, and interaction components. First, we introduce a convolution filter for capturing seasonal effects, which significantly reduces the complexity of FBM-L while achieving even better results. For the trend block, we integrate the strengths of FBM-NL and FBM-NP, enhancing both efficiency and performance through patching applied to MLP and Transformer architectures. We find that Transformer architecture is generally unnecessary, with the Traffic dataset being the only exception. For all other datasets, a single-layer projection is sufficient to replace stacked of attention layers, yielding better performance. Consequently, we use a Transformer backbone for the Traffic dataset and an MLP backbone for the remaining datasets in the trend block,

respectively. Thus, FBM-S outperforms the other three FBM variants in nearly all cases, achieving state-of-the-art performance in most scenarios. We observe that interaction effects hold a value, but play a relatively minor role in long-term TSF, while have a more significant impact in short-term TSF, which will be discussed in the next Section. The interaction block is effective for the Electricity, Traffic, ETTm1, ETTm2, and WTH when interaction masking is applied. Additionally, we observe that multi-scale down-sampling is effective for high-granularity datasets such as ETTm1. The same findings are observed for short-term TSF. Detail discussion can be found in the ablation studies in Section VI-E.

C. Short-term TSF Results

In Table III, we compare our proposed FBM-variants with other baselines on four PEMS datasets for STSF. The PEMS datasets have high granularity, with data recorded at 5-minute intervals. As a result, FBM-S shows a notably greater performance improvement over the other three FBM variants across all four PEMS datasets by involving the interaction block. This can be attributed to two main reasons. First, the forecast horizon is shortened for $L = (12, 24, 48, 96)$, and

TABLE V: Efficiency Analysis on the PEMS08 Dataset (Batch Size = 64, $T = 336$, $L = 96$)

	FBM-S	FBM-L	FBM-NL	FBM-NP	NLinear [48]	PatchTST [24]	TimeMixer [17]	iTransformer [35]	FiLM [9]	TimesNet [16]
Training time (s)	10.94	4.39	23.34	13.50	2.38	33.53	7.95	4.94	134.95	432.95
Memory (KMiB)	13.06	9.55	10.11	15.61	0.11	20.04	2.63	2.95	43.41	5.28
GFLOPs	172.15	59.31	913.71	141.31	0.35	187.87	36.40	53.90	-	41786.75

TABLE VI: FBM-S Model Configuration Details in the Trend, Seasonal, and Interaction Blocks. Results are measured on the PEMS08 dataset with a batch size of 64 with $T = 336$ and $L = 96$.

	Trend Block (MLP)	Trend Block (MLP+Patch)	Trend Block (Transformer+Patch)	Interaction Block (Transformer)	Seasonal Backbone
Hyperparameter	$h_1 = h_2 = 1440$	$P = 14, h_1 = 256, h_2 = 1440$	$P = 14, h_1 = h_2 = 256, K = 3$	$h_3 = 512, K = 3, C_1 = 24$	-
Initial Projection	$\frac{1}{4} \times \frac{T^2}{2} \times h_1 = 20.32M$	$\frac{1}{4} \times \frac{T^2}{2P} \times h_1 = 0.26M$	$\frac{1}{4} \times \frac{T^2}{2P} \times h_1 = 0.26M$	$(24 \times \frac{T}{2}) \times h_3 = 2.06M$	-
Intermediate Layer	$h_1 \times h_2 = 2.07M$	$(h_1 \times P) \times h_2 = 5.16M$	$h_1 \times h_1 \times 4 \times 3 + h_1 \times h_2 \times 2 \times 3 = 1.18M$	$h_3 \times h_3 \times 6 \times 3 = 4.71M$	0.05M
Final Projection	$h_2 \times L = 0.14M$	$h_2 \times L = 0.14M$	$(h_1 \times P) \times L = 0.17M$	$h_3 \times L = 0.05M$	-
Total Parameter	22.53M	5.56M	1.61M	6.82M	0.05M
FLOPs(G)(Batch Size=64)	245.16	96.96	223.67	74.49	0.70

h_1 and h_2 refer to the hidden states within trend block, h_3 refer to the hidden states within interaction block. P refers to the number of patches, K refers to the number of attention stacks, and C_1 and C_2 refers to the input and output interaction mask.

second, the data are recorded at 5-minute intervals. Thus, the actual forecast horizon in real world time is very short. The interaction effects become much more pronounced over short periods, as previously mentioned. The trend and seasonal effects are primarily driven by endogenous temporal patterns within each time series, whereas the interaction effects are influenced by exogenous dependencies across multivariate time series. It is worth mentioning that centralization and the interaction mask also play an important role in improving the significance of the interaction block. We use an input mask with $C_1 = 24$ and an output mask with $C_2 = L$. The input mask helps remove outdated redundant temporal information for interaction effects. It also helps improve the efficiency of the initial projection. Centralization helps the model determine whether the recent time series segment corresponds to a high-peak, off-peak, or normal state period for each variate. On the other hand, the proposed multi-scale down-sampling and patching in the trend block are also effective for short-term TSF. Finally, we observe that FBM-S achieves SOTA performance all the time. Detail discussion can be found in the ablation studies in Section VI-E.

In Table IV, we compare our proposed FBM-S with other baselines on the M4 dataset across different sampling frequencies. Since M4 is a univariate dataset, we won't use the interaction block. We follow the official setting used in TimeMixer [17] where the input length is set to twice the forecast horizon. As mentioned, the forecast horizons are 6 for yearly, 8 for quarterly, 18 for monthly, 13 for weekly, and 14 for daily and 48 for hourly, respectively. Given the relatively short input lengths, patching becomes unnecessary. We observe that when the forecast horizon increases, our method becomes increasingly competitive and achieves the best overall performance. This is because the number of meaningful frequency levels is proportional to the input series length; more frequency levels lead to better results. All experiments are conducted using the same random seed and the fixed hyperparameters listed in Table I to ensure the best reproducibility of the reported results. This means that we do not search for and report the best-case results of our model.

D. Efficiency Analysis

Table V shows the computational efficiency of our method with baseline methods, reporting average training time per epoch, memory usage, and FLOPs. Table VI specifies the default configuration of each block, including layer architecture, number of parameters, and FLOPs. All evaluations are conducted on the PEMS08 dataset with $T = 336$, $L = 96$, and a batch size of 64.

In Table V, FBM-S demonstrates good overall efficiency and achieves the best performance among the existing methods. Given that TimeMixer and iTransformer are among the most efficient nonlinear methods, FBM-S introduces only a small increase in complexity but is more efficient than all the other nonlinear methods. Moreover, FBM-S is even more efficient than other non-linear FBM variants, such as FBM-NL and FBM-NP.

In Table VI, we show the detailed configuration of each layer within each block, where each block, except for the seasonal block, can be decomposed into an initial projection, the intermediate layer, and a final projection layer. The intermediate layer are either a single projection layer in MLP backbone or stacks of attention layers in attention backbone. In the Trend block, the patching technique substantially improves the overall efficiency of the MLP-based architecture. We also observe that a three-layer MLP with patching achieves lower FLOPs compared to Transformer-based methods. The speed is also faster since the trend block with MLP requires only three rounds of matrix multiplication, whereas the trend block with a transformer requires twenty-four rounds of matrix multiplication. The results demonstrate that both seasonal block (MLP + patch) and interaction block achieve high efficiency, as evidenced by low FLOPs.

This further highlights the importance of time-frequency features. By slightly increasing the complexity of the initial layer, we can reduce that of the downstream layers. For example, FBM-NP outperforms PatchTST not only in predictive performance but also in computational efficiency as we use fewer patches. The experiments are conducted on a NVIDIA H100 GPU and Intel Xeon Gold CPU.

TABLE VII: Ablation Study I: Enhancing the Trend (T) Block with Seasonal (S) and Interaction (I) Blocks in LTSF. Masking (M) and Centralization (C) are applied in interaction block.

Model		T		S+T		S+T+I(C)		S+T+I(C+M)	
Error		MSE	MAE	MSE	MAE	MSE	MAE	MSE	MAE
ETTh1	96	0.367	0.392	0.363	0.389	0.366	0.390	<u>0.365</u>	<u>0.389</u>
	192	0.403	0.411	0.399	0.409	0.401	0.411	<u>0.399</u>	<u>0.409</u>
	336	0.418	0.420	0.402	0.413	0.408	0.417	<u>0.403</u>	<u>0.413</u>
	720	0.417	0.439	0.403	0.433	0.409	0.436	<u>0.403</u>	<u>0.433</u>
ETTm1	96	0.290	0.346	0.278	0.332	0.383	0.338	0.278	0.332
	192	0.330	0.371	0.319	0.359	0.322	0.363	0.317	0.358
	336	0.362	0.390	0.359	0.384	0.362	0.390	0.356	0.382
	720	0.415	0.421	0.413	0.419	0.415	0.419	0.412	0.418

TABLE VIII: Ablation Study II: Removing the Interaction Block, Centralization (C) and Masking (M) Techniques within the Interaction Block in STSF.

Model		S+T+I(C+M)		S+T+I(M)		S+T+I(C)		S+T	
Error		MSE	MAE	MSE	MAE	MSE	MAE	MSE	MAE
PEMS08	12	0.055	0.147	<u>0.056</u>	<u>0.148</u>	0.057	0.150	0.058	0.151
	24	0.064	0.157	<u>0.065</u>	<u>0.159</u>	0.066	0.159	0.069	0.163
	48	0.073	0.167	<u>0.076</u>	<u>0.170</u>	0.077	0.171	0.085	0.178
	96	0.083	0.177	<u>0.088</u>	<u>0.181</u>	0.088	0.181	0.102	0.194

E. Ablation Studies

We conducted seven ablation studies for designs for time-frequency features. We first analyze the network's decomposition into trend, seasonal, and interaction blocks. In Table VII, we first observe that combining the trend block with the seasonal block consistently outperforms using the trend block alone. This convolutional filter encourages the output features to exhibit seasonal characteristics, which enhances the robustness of the model.

We then observe that the interaction block is generally less effective in LTSF, as adding the interaction block with masking makes only a small difference. Additionally, applying a mask with $C_1 = C_2 = 48$ consistently outperforms the setting without such a mask. Including interaction mechanisms tends to degrade performance on ETTh1 but improves performance on ETTm2 when the data granularity changes from hourly to 15-minute intervals. This further highlights that the interaction effect is more important over shorter time periods. This explains why FBM-S shows a significant performance improvement over the other three FBM variants in STSF. We then conduct a more detailed analysis of the effects of the interaction block on the PEMS dataset.

In Table VIII, we further evaluate the impact of adding the interaction block on PEMS08, as well as two design choices: centralization and masking. We find that removing the interaction block leads to a significant drop in performance on the PEMS08 dataset. This can be attributed to the shorter forecast horizon L and the high granularity of the 5-minute sampling frequency in the PEMS dataset. These results suggest that while both dependent channel modeling and independent channel modeling are effective, dependent modeling plays an increasingly important role in the short term. The masking and centralization techniques have also been proven effective in the interaction block. Centralizing the final patch of time-frequency features allows the model to

TABLE IX: Ablation Study III: Effects of the Input Interaction Mask Range (C_1) with $C_2 = L$ in STSF.

Parameter		$C_1 = 24$		$C_1 = 48$		$C_1 = 96$		$C_1 = 336$	
Error		MSE	MAE	MSE	MAE	MSE	MAE	MSE	MAE
PEMS08	12	0.055	0.147	<u>0.056</u>	<u>0.148</u>	0.056	0.150	0.057	0.150
	24	0.064	0.157	<u>0.064</u>	<u>0.157</u>	0.065	0.159	0.066	0.159
	48	0.073	0.167	<u>0.074</u>	<u>0.168</u>	0.074	0.168	0.077	0.171
	96	0.083	0.177	0.082	0.175	<u>0.083</u>	<u>0.176</u>	0.088	0.181

TABLE X: Ablation study IV: The Effects of the Output Interaction Mask Range (C_2) with $C_1 = 24$ in LTSF

Parameter		$C_2 = 0$		$C_2 = 24$		$C_2 = 48$		$C_2 = 336$	
Error		MSE	MAE	MSE	MAE	MSE	MAE	MSE	MAE
Electricity	96	<u>0.128</u>	<u>0.220</u>	0.127	0.220	0.129	0.222	0.129	0.222
	192	<u>0.144</u>	<u>0.237</u>	0.144	0.237	0.148	0.240	0.151	0.242
	336	<u>0.162</u>	<u>0.255</u>	0.161	0.254	0.164	0.256	0.168	0.261
	720	<u>0.196</u>	<u>0.286</u>	0.195	0.285	0.195	0.285	0.201	0.289

better interpret whether the current segment of the time series corresponds to a high-peak or low-peak period. This, in turn, enhances the downstream interaction mapping by providing a clearer understanding of the recent time series intensity level. The masking allows the model to incorporate only the most relevant time-frequency features while removing redundant information.

In Table IX, we then investigate the impact of the input interaction mask range on the PEMS dataset. The results show that using a longer range of time-frequency features does not improve performance; instead, it gradually leads to performance degradation. This highlights that the interaction effects primarily arise from the most recent time-frequency features. For example, the best results are achieved with $C_1 = 24$ and $C_2 = 48$. Using the full time-frequency representation leads to the worst performance, as it includes excessive and unnecessary information for interaction effects. However, longer-range time-frequency representations are useful for capturing trend and seasonal effects. This underscores the necessity of separating the trend, seasonal and interaction components, with masking applied specifically in the interaction block.

In Table X, we evaluate the effect of varying the output interaction mask range on the Electricity dataset for LTSF. This analysis is motivated by our earlier reasoning that the interaction effects are more effective in a short period. By comparing the first and second columns, we observe that the interaction block provides a small performance improvement only when an output mask is applied. With the input mask C_1 fixed at 24, we find that the best performance is achieved when the output mask C_2 is also set to 24. Increasing or decreasing the value will lead to worse results.

In Table XI, we evaluate the impact of multi-scale down-sampling and find that it is particularly effective for high-granularity data. Here, d_0 refers to the original time-frequency input, d_1 denotes down-sampled input once, and d_2 denotes down-sampled input twice. We evaluated the performance in different combinations and observed that using d_1 yields the best results. This suggests that moderate down-sampling can enhance the quality of time-frequency features, as excessively high resolution may lead to overfitting, while a lower resolu-

TABLE XI: Ablation Study V: Effects of the Multi-Scale Down-Sampling on PEMS08.

Model		d_0		d_1		$d_0 + d_1$		$d_0 + d_1 + d_2$	
Error		MSE	MAE	MSE	MAE	MSE	MAE	MSE	MAE
PEMS08	12	0.056	0.148	0.055	0.147	0.057	0.147	0.057	0.149
	24	0.064	0.158	0.064	0.157	0.064	0.158	0.064	0.155
	48	0.075	0.170	0.073	0.167	0.074	0.168	0.074	0.168
	96	0.083	0.177	0.083	0.177	0.083	0.176	0.084	0.176

TABLE XII: Ablation Study VI: Effects of Patching with Centralization (C) Technique in Trend Block

Trend Block		Patch(C)		Patch		w/o Patch	
Error		MSE	MAE	MSE	MAE	MSE	MAE
Weather	96	0.147	0.196	0.152	0.199	0.152	0.199
	192	0.189	0.238	0.194	0.241	0.194	0.241
	336	0.238	0.276	0.245	0.283	0.244	0.282
	720	0.311	0.328	0.317	0.335	0.316	0.332

tion helps improve generalization.

In Table XII, We evaluate the effects of patching with centralization technique within trend block. We find that applying patching together with centralization improves performance compared to using the entire time-frequency features. Notably, as discussed in Section VI-D, patching also significantly enhances computational efficiency. Thus, the combination of patching and centralization improves forecasting accuracy while simultaneously reducing overall model complexity. This is because centralization helps the model better capture the overall trend within a short temporal window, leading to improved performance.

In Table XIII, we first compare MLP-based and Transformer-based networks for patched time-frequency features. We observe that the MLP-based network consistently outperforms the Transformer-based network across those datasets, with the only exception being the Traffic dataset. In Section VI-D, we also find that the MLP-based architecture is more efficient than the transformer architecture. These findings underscore the superior efficiency and performance of the MLP-based network in modeling time-frequency features for trend effects. Secondly, we further test the effect of adding an activation function after the initial projection layer of the patched time-frequency features. We observe that the model achieves better performance with the activation function. This improvement is attributed to the activation function helping the model capture nonlinear trend effects more effectively. Although the downstream intermediate layer includes activation functions, incorporating an additional activation function immediately after the initial projection also brings benefits and improve robustness. This enhancement is more obvious in MLP-based network than Transformer-based network.

In Table XIV, we analyze different experimental settings. We compare performance using a train/validation/test split of 0.7/0.1/0.2 and an input length of $T = 96$, as adopted by many previous works. We find that using an input length of 336 consistently yields better results, and using a larger training set improves performance, thus we will consider use a larger training set in the future work.

TABLE XIII: Ablation Study VII : Linear VS Non-Linear Initial Projection and MLP vs Transformer Networks.

Model		Linear Proj (MLP)		Non-Linear Proj (MLP)		Linear Proj (Transformer)		Non-Linear Proj (Transformer)	
Error		MSE	MAE	MSE	MAE	MSE	MAE	MSE	MAE
PEMS08	12	0.057	0.149	0.055	0.147	0.058	0.152	0.057	0.150
	24	0.066	0.161	0.064	0.157	0.065	0.159	0.065	0.158
	48	0.075	0.169	0.073	0.167	0.075	0.168	0.075	0.168
	96	0.086	0.180	0.083	0.177	0.084	0.177	0.084	0.178
Electricity	96	0.127	0.220	0.127	0.220	0.126	0.220	0.127	0.220
	192	0.145	0.237	0.144	0.237	0.144	0.237	0.145	0.237
	336	0.163	0.256	0.161	0.254	0.162	0.255	0.161	0.254
	720	0.197	0.287	0.195	0.285	0.197	0.287	0.195	0.285

TABLE XIV: Experiment Settings for Different Input Length and Train/Vali/Test Split

Dataset	L	Electricity				Traffic			
		96	192	336	720	96	192	336	720
Ours:(T=336, 0.65/0.15/0.2)	MSE	0.127	0.144	0.161	0.195	0.357	0.382	0.393	0.430
	MAE	0.220	0.237	0.254	0.285	0.246	0.257	0.263	0.285
(T=96, 0.65/0.15/0.2)	MSE	0.138	0.153	0.170	0.206	0.408	0.420	0.432	0.462
	MAE	0.233	0.247	0.265	0.297	0.257	0.269	0.276	0.291
(T=336, 0.7/0.1/0.2)	MSE	0.124	0.141	0.157	0.191	0.346	0.367	0.382	0.414
	MAE	0.217	0.234	0.251	0.282	0.244	0.252	0.260	0.281

F. Why Rolling Window in Seasonal Block?

Here, we aim to understand why using a sliding window or a patched projection can be advantageous. This is because the original Fourier basis follows sinusoidal patterns, and when a window filter slides over the time domain, it can automatically capture seasonal features. The same applies to patched projection, which can be regarded as a windowed filter with a stride equal to the patch length, inherently extracting meaningful features over a specific period. To support this claim, we visualize the heatmaps of the learned weights of FBM-L on the Electricity dataset in Figure 5, to better understand how FBM-L captures the relationships between input time-frequency features and the output time series. Specifically, we decompose the weight matrix \mathbf{W} into L time-specific components, where each \mathbf{W}_i represents the influence of the time-frequency features on the i -th time step of the predicted output time series $\hat{\mathbf{Y}}$. The heatmaps resemble Fourier basis patterns but differ in finer details, indicating that it allows the model to remove noise across both the time and frequency domains. We also observe that when heatmaps \mathbf{W}_i gradually shift along i , they produce similar patterns over time. This indicates that the similarities captures coarse seasonal features, while the finer differences correspond to residual trend effects. This observation suggests that the weights can be shared via convolution, allowing a single weight matrix \mathbf{W} to capture the overall coarse seasonal structure. The remaining blocks in FBM-S can then focus on generating finer patterns, resulting in a more efficient and robust prediction.

G. Case Study

In Figure 6, we present two case studies illustrating the forecast performance of our model compared to TimeMixer and iTransformer on the PEMS08 dataset, along with visualizations of the trend, seasonal, and interaction decompositions. These two models represent the state-of-the-art baselines for

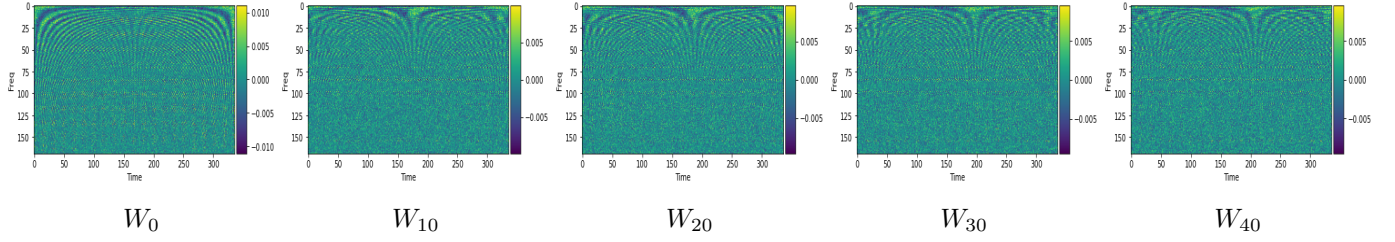


Fig. 5: Visualization of the Weights W_0 , W_{10} , W_{20} , W_{30} , and W_{40} of FBM-L on the Electricity Dataset. Each W_i represents the influence of time-frequency features on the i -th time step of the predicted output \hat{Y} . The x -axis denotes time, and the y -axis denotes frequency.

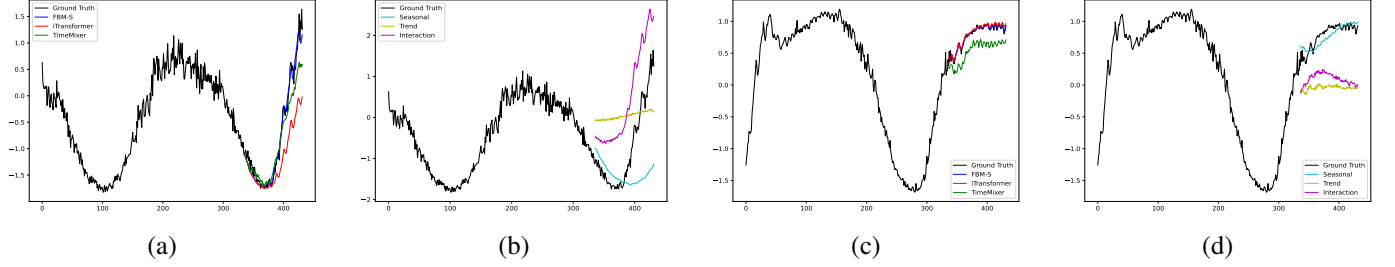


Fig. 6: Forecasting Performance Visualization: Two Case Studies on PEMS08. (a) and (b) form the first case, and (c) and (d) form the second case. (a) and (c) compare FBM-S with TimeMixer and iTransformer, while (b) and (d) show each forecasting component: trend, seasonal, and interaction block.

channel independent and channel dependent modeling, respectively. First, Figures 6a and 6c show that our model achieves better forecasting results than both baselines. Second, Figures 6b and 6d explain why our decomposition works better. We observe that the seasonal, trend, and interaction components capture meaningful corresponding patterns. This suggests that the model effectively leverages different modalities: the trend and seasonal signals from endogenous factors, as well as interaction effects from exogenous variables, combined with both time-frequency space.

In Figure 6b and Figure 6c, we find that the model generates more prominent features from the seasonal and interaction backbones, indicating that these components play a more important role through backpropagation in STSF. On the other hand, we observe the trend component tends to stay close to the zero axis, implying that it try to refined mistakes made by the other blocks. For example, the other baselines, shown in Figures 6a and 6b, do not accurately capture the distinct effects. However, through fine-tuning the decomposition from different modalities, our model produces a more precise and reliable overall forecast. Specifically, the trend block generates outputs greater than zero in Figure 6b, while the interaction block produces adjusted values in Figure 6d, which help correct the mispredictions made by other baselines in Figures 6a and 6b, respectively. This synergetic cooperation enables the model to achieve significantly better forecast results.

H. Distribution of Frequency Spectrum

To better understand the data characteristics, we visualize the distribution of the input frequency spectrum in Figure 7, which helps explain the experimental results and justify

the hyperparameter selections. The visualization shows the mean of the input frequency spectrum along with its 95 percent confidence interval for different datasets. In Table II and Table III, we first observe that FBM-NL and FBM-NP perform similarly across most datasets, due to both being nonlinear models. However, FBM-NL generally outperforms FBM-NP, except on the Traffic dataset. This exception is due to the fact that the frequency spectrum distribution of the Traffic dataset shows the least diversity and variation, making it more suitable for a transformer-based architecture. Thus, we can conclude that the Transformer-based architecture is more prone to overfitting in datasets where the frequency spectrum is highly diverse and variable. Secondly, FBM-L and FBM-NL show significant performance differences on the ETTh dataset compared to the others, likely due to a common underlying issue. The ETTh dataset exhibits the most diverse frequency spectrum and the greatest variation, indicating a higher proportion of noise signals in ETTh1 and ETTh2 than in the other datasets. As a result, a simpler linear model is more suitable for capturing the effects in ETTh datasets.

Figure 7 shows that trend effects generally appear at low-frequency levels, seasonal effects typically occur at intermediate frequencies, and noise signals usually arise high-frequency levels. This explains why the Fourier transform is beneficial for TSF, as it hierarchically separates various effects, with specific effects (e.g., hourly, daily) aligning with their corresponding frequency levels. For instance, Figure 7 shows consistently high energy at multiples of 14 across all hourly-level datasets: ETTh1, ETTh2, Electricity, and Traffic. This is attributed to the day effect falling into these frequency levels, given the repeating cycle of 24 with a look-back window of 336.

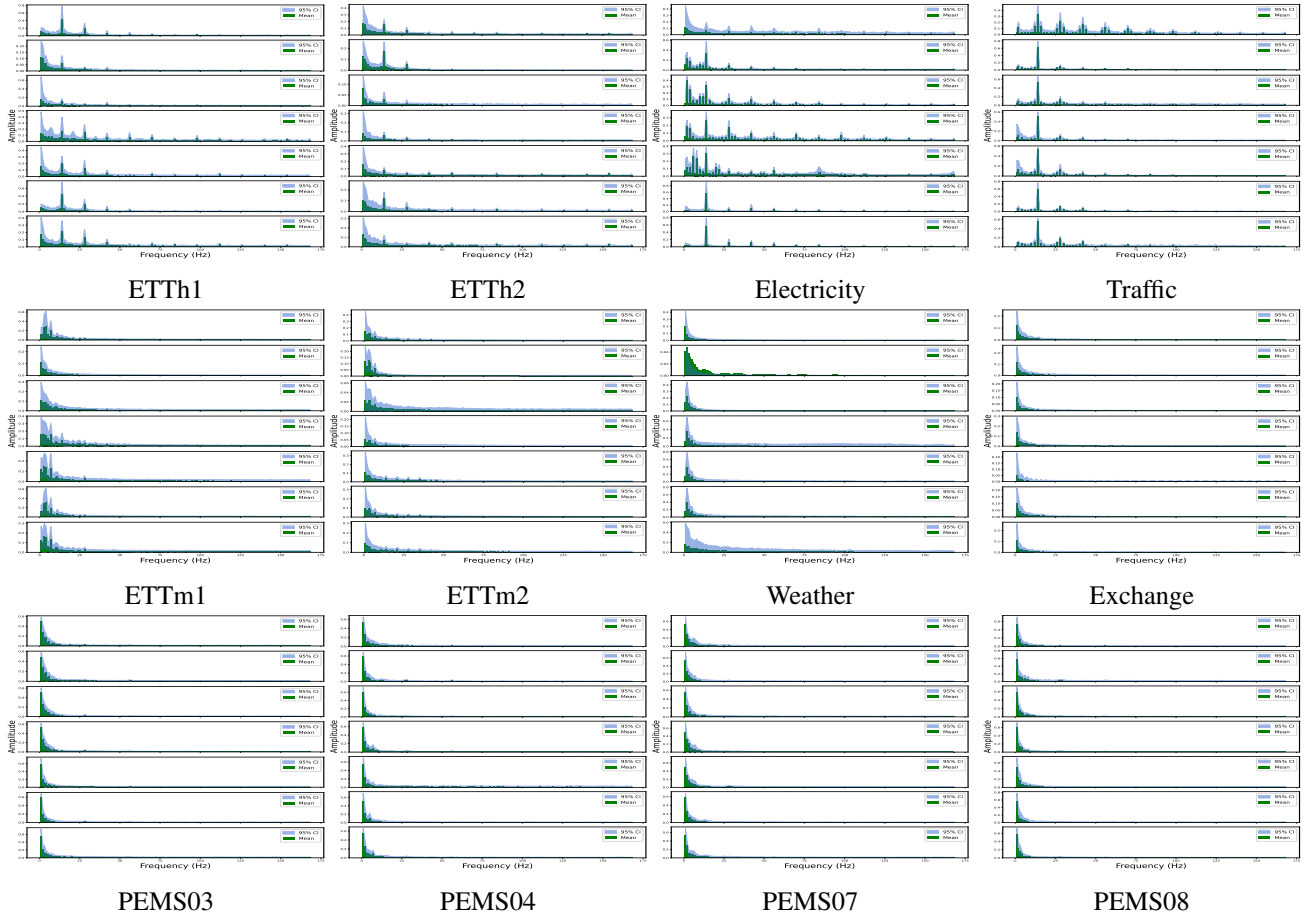


Fig. 7: Frequency Spectrum Distribution of the Last Seven Dimensions on Twelve Datasets. Here, the green bars represent the mean values, while the light blue shaded area indicates the 95 percentage confidence interval.

Variations in the frequency spectrum also indicate that the spectral landscape is highly sensitive to the characteristics of the underlying data. For hourly-level datasets, the frequency spectrum are more diverse, whereas minute-level datasets tend to exhibit much more energy gathering in lower frequency range. For instance, the frequency spectrum of ETTm1 and ETTm2 are shifted to the left compared to those of ETTh1 and ETTh2. This shift effectively shortens the forecast horizon in the time domain, resulting in reduced noise in these data. This helps explain why non-Linear network performs slightly better than linear network on ETTm1 when the granularity changes. This also applies to the other datasets. For example, the PEMS dataset, which has the highest data granularity at a five-minute level, exhibits a frequency spectrum that is even more concentrated at lower frequency levels. These findings support our initial hypothesis: simply providing the real and imaginary parts is not sufficient, as frequency interpretations are ambiguous when changes in data granularity or sequence length alter the meaning of those components. In conclusion, when a dataset contains a large proportion of noise and limited data, simpler models tend to perform better; vice versa.

VII. CONCLUSION AND FUTURE WORK

We make the first attempt to theoretically and empirically discuss several issues related to existing Fourier-based

methods for time series forecasting from the perspective of basis functions. Our insights and findings disclose two issues commonly appearing in existing studies: inconsistent starting cycles and inconsistent series length issues. Thus, we address the aforementioned issue by including the basis functions, retaining time-domain information. This allows the model to take advantage of both time and frequency modality. Therefore, we propose a new time-frequency framework, namely Fourier Basis Mapping (FBM). Extensive experiments empirically verify the effectiveness of the FBM approach, to enhance various types of mapping networks through three FBM variants: FBM-L, FBM-NL, FBM-NP. Then, we further propose a new synergistic FBM model, referred to as FBM-S, which further enhances the SOTA performance in both short-term and long-term TSF tasks. This model decomposes the effects into three components: trend, seasonal, and interaction, combining the strengths of independent-channel and dependent-channel modeling. We also propose several useful techniques for modeling time-frequency features, which are validated by seven ablation studies conducted on both tasks. However, there is one limitation of our methods that the input sequence length should not be too short, as the meaningful Fourier basis are bounded by input sequence length. Time-frequency features hold great potential for future time series

analysis tasks. The FBM framework offers a new pathway for time-frequency learning approaches. In the future, we will further extend its application to other domains, such as anomaly detection.

REFERENCES

- [1] S. Hochreiter and J. Schmidhuber, "Long short-term memory," *Neural Computation*, vol. 9, no. 8, pp. 1735–1780, 1997.
- [2] J. Chung, C. Gulcehre, K. Cho, and Y. Bengio, "Empirical evaluation of gated recurrent neural networks on sequence modeling," *arXiv preprint arXiv:1412.3555*, 2014.
- [3] S. S. Rangapuram, M. W. Seeger, J. Gasthaus, L. Stella, Y. Wang, and T. Januschowski, "Deep state space models for time series forecasting," *Neural Information Processing Systems Conference*, vol. 31, 2018.
- [4] S. Chang, Y. Zhang, W. Han, M. Yu, X. Guo, W. Tan, X. Cui, M. Witbrock, M. A. Hasegawa-Johnson, and T. S. Huang, "Dilated recurrent neural networks," *Neural Information Processing Systems Conference*, vol. 30, 2017.
- [5] X. Liu and Z. Lin, "Impact of covid-19 pandemic on electricity demand in the uk based on multivariate time series forecasting with bidirectional long short term memory," *Energy*, vol. 227, p. 120455, 2021.
- [6] T. Gangopadhyay, S. Y. Tan, Z. Jiang, R. Meng, and S. Sarkar, "Spatiotemporal attention for multivariate time series prediction and interpretation," in *IEEE International Conference on Acoustics, Speech and Signal Processing*. IEEE, 2021, pp. 3560–3564.
- [7] Y. Jia, Y. Lin, X. Hao, Y. Lin, S. Guo, and H. Wan, "WITRAN: Water-wave information transmission and recurrent acceleration network for long-range time series forecasting," in *Neural Information Processing Systems Conference*, 2023.
- [8] D. Salinas, V. Flunkert, J. Gasthaus, and T. Januschowski, "DeepAR: Probabilistic forecasting with autoregressive recurrent networks," *International Journal of Forecasting*, vol. 36, no. 3, pp. 1181–1191, 2020.
- [9] T. Zhou, Z. Ma, Q. Wen, L. Sun, T. Yao, W. Yin, R. Jin *et al.*, "FiLM: Frequency improved legendre memory model for long-term time series forecasting," *Neural Information Processing Systems Conference*, vol. 35, pp. 12 677–12 690, 2022.
- [10] D. Luo and X. Wang, "ModernTCN: A modern pure convolution structure for general time series analysis," in *International Conference on Learning Representations*, 2024.
- [11] S. Bai, J. Z. Kolter, and V. Koltun, "An empirical evaluation of generic convolutional and recurrent networks for sequence modeling," *arXiv preprint arXiv:1803.01271*, 2018.
- [12] M. Liu, A. Zeng, M. Chen, Z. Xu, Q. Lai, L. Ma, and Q. Xu, "SCINet: Time series modeling and forecasting with sample convolution and interaction," *Neural Information Processing Systems Conference*, vol. 35, pp. 5816–5828, 2022.
- [13] H. Wang, J. Peng, F. Huang, J. Wang, J. Chen, and Y. Xiao, "MICN: Multi-scale local and global context modeling for long-term series forecasting," in *International Conference on Learning Representations*, 2022.
- [14] J.-Y. Franceschi, A. Dieuleveut, and M. Jaggi, "Unsupervised scalable representation learning for multivariate time series," *Neural Information Processing Systems Conference*, vol. 32, 2019.
- [15] R. Sen, H.-F. Yu, and I. S. Dhillon, "Think globally, act locally: A deep neural network approach to high-dimensional time series forecasting," *Neural Information Processing Systems Conference*, vol. 32, 2019.
- [16] H. Wu, T. Hu, Y. Liu, H. Zhou, J. Wang, and M. Long, "TimesNet: Temporal 2d-variation modeling for general time series analysis," in *International Conference on Learning Representations*, 2022.
- [17] S. Wang, H. Wu, X. Shi, T. Hu, H. Luo, L. Ma, J. Y. Zhang, and J. Zhou, "Timemixer: Decomposable multiscale mixing for time series forecasting," *arXiv preprint arXiv:2405.14616*, 2024.
- [18] P. Tang and W. Zhang, "Unlocking the power of patch: Patch-based mlp for long-term time series forecasting," in *AAAI*, vol. 39, no. 12, 2025, pp. 12 640–12 648.
- [19] S.-A. Chen, C.-L. Li, N. Yoder, S. O. Arik, and T. Pfister, "Tsmixer: An all-mlp architecture for time series forecasting," *arXiv preprint arXiv:2303.06053*, 2023.
- [20] B. N. Oreshkin, D. Carpo, N. Chapados, and Y. Bengio, "N-BEATS: Neural basis expansion analysis for interpretable time series forecasting," in *International Conference on Learning Representations*, 2019.
- [21] C. Challu, K. G. Olivares, B. N. Oreshkin, F. G. Ramirez, M. M. Canseco, and A. Dubrawski, "N-HiTS: Neural hierarchical interpolation for time series forecasting," in *AAAI Conference on Artificial Intelligence*, vol. 37, no. 6, 2023, pp. 6989–6997.
- [22] K. Yi, Q. Zhang, W. Fan, S. Wang, P. Wang, H. He, N. An, D. Lian, L. Cao, and Z. Niu, "Frequency-domain mlps are more effective learners in time series forecasting," in *Neural Information Processing Systems Conference*, 2023.
- [23] A. Vaswani, N. Shazeer, N. Parmar, J. Uszkoreit, L. Jones, A. N. Gomez, L. Kaiser, and I. Polosukhin, "Attention is all you need," *Neural Information Processing Systems Conference*, vol. 30, 2017.
- [24] Y. Nie, N. H. Nguyen, P. Sinthong, and J. Kalagnanam, "A time series is worth 64 words: Long-term forecasting with transformers," in *International Conference on Learning Representations*, 2022.
- [25] Z. Ni, H. Yu, S. Liu, J. Li, and W. Lin, "BasisFormer: Attention-based time series forecasting with learnable and interpretable basis," in *Neural Information Processing Systems Conference*, 2023.
- [26] H. Zhou, S. Zhang, J. Peng, S. Zhang, J. Li, H. Xiong, and W. Zhang, "Informor: Beyond efficient transformer for long sequence time-series forecasting," in *AAAI Conference on Artificial Intelligence*, vol. 35, no. 12, 2021, pp. 11 106–11 115.
- [27] H. Wu, J. Xu, J. Wang, and M. Long, "Autoformer: Decomposition transformers with auto-correlation for long-term series forecasting," *Advances in Neural Information Processing Systems*, vol. 34, pp. 22 419–22 430, 2021.
- [28] S. Liu, H. Yu, C. Liao, J. Li, W. Lin, A. X. Liu, and S. Dustdar, "Pyraformer: Low-complexity pyramidal attention for long-range time series modeling and forecasting," in *International conference on learning representations*, 2021.
- [29] Y. Zhang and J. Yan, "Crossformer: Transformer utilizing cross-dimension dependency for multivariate time series forecasting," in *International Conference on Learning Representations*, 2022.
- [30] H. Cao, Z. Huang, T. Yao, J. Wang, H. He, and Y. Wang, "InParformer: evolutionary decomposition transformers with interactive parallel attention for long-term time series forecasting," in *AAAI Conference on Artificial Intelligence*, vol. 37, no. 6, 2023, pp. 6906–6915.
- [31] K. Fu, H. Li, and X. Shi, "An encoder–decoder architecture with fourier attention for chaotic time series multi-step prediction," *Applied Soft Computing*, p. 111409, 2024.
- [32] Z. Zhang, Y. Han, B. Ma, M. Liu, and Z. Geng, "Temporal chain network with intuitive attention mechanism for long-term series forecasting," *IEEE Transactions on Instrumentation and Measurement*, 2023.
- [33] D. Cao, F. Jia, S. O. Arik, T. Pfister, Y. Zheng, W. Ye, and Y. Liu, "Tempo: Prompt-based generative pre-trained transformer for time series forecasting," *arXiv preprint arXiv:2310.04948*, 2023.
- [34] P. Chen, Y. Zhang, Y. Cheng, Y. Shu, Y. Wang, Q. Wen, B. Yang, and C. Guo, "Pathformer: Multi-scale transformers with adaptive pathways for time series forecasting," *arXiv preprint arXiv:2402.05956*, 2024.
- [35] Y. Liu, T. Hu, H. Zhang, H. Wu, S. Wang, L. Ma, and M. Long, "iTrans-former: Inverted transformers are effective for time series forecasting," in *International Conference on Learning Representations*, 2024.
- [36] X. Qiu, X. Wu, Y. Lin, C. Guo, J. Hu, and B. Yang, "Duet: Dual clustering enhanced multivariate time series forecasting," *arXiv preprint arXiv:2412.10859*, 2024.
- [37] Y. Liu, G. Qin, X. Huang, J. Wang, and M. Long, "Timer-xl: Long-context transformers for unified time series forecasting," *arXiv preprint arXiv:2410.04803*, 2024.
- [38] J. Fan, Z. Wang, D. Sun, and H. Wu, "Sepformer-based models: More efficient models for long sequence time-series forecasting," *IEEE Transactions on Emerging Topics in Computing*, 2022.
- [39] T. Zhou, Z. Ma, Q. Wen, X. Wang, L. Sun, and R. Jin, "Fedformer: Frequency enhanced decomposed transformer for long-term series forecasting," in *International Conference on Machine Learning*. PMLR, 2022, pp. 27 268–27 286.
- [40] Q. Huang, L. Shen, R. Zhang, S. Ding, B. Wang, Z. Zhou, and Y. Wang, "CrossGNN: Confronting noisy multivariate time series via cross interaction refinement," in *Neural Information Processing Systems Conference*, 2023.
- [41] K. Yi, Q. Zhang, W. Fan, H. He, L. Hu, P. Wang, N. An, L. Cao, and Z. Niu, "FourierGNN: Rethinking multivariate time series forecasting from a pure graph perspective," *arXiv preprint arXiv:2311.06190*, 2023.
- [42] A. Cini, I. Marisca, D. Zambon, and C. Alippi, "Graph deep learning for time series forecasting," *arXiv preprint arXiv:2310.15978*, 2023.
- [43] A. Sriramulu, N. Fourier, and C. Bergmeir, "Adaptive dependency learning graph neural networks," *Information Sciences*, vol. 625, pp. 700–714, 2023.
- [44] M. Jin, Y. Zheng, Y.-F. Li, S. Chen, B. Yang, and S. Pan, "Multivariate time series forecasting with dynamic graph neural odes," *IEEE Transactions on Knowledge and Data Engineering*, vol. 35, no. 9, pp. 9168–9180, 2022.

- [45] K. Alkilane, Y. He, and D.-H. Lee, "Mixmamba: Time series modeling with adaptive expertise," *Information Fusion*, vol. 112, p. 102589, 2024.
- [46] Z. Wang, F. Kong, S. Feng, M. Wang, X. Yang, H. Zhao, D. Wang, and Y. Zhang, "Is mamba effective for time series forecasting?" *Neurocomputing*, vol. 619, p. 129178, 2025.
- [47] C. Zeng, Z. Liu, G. Zheng, and L. Kong, "Cmamba: Channel correlation enhanced state space models for multivariate time series forecasting," *arXiv preprint arXiv:2406.05316*, 2024.
- [48] A. Zeng, M. Chen, L. Zhang, and Q. Xu, "Are transformers effective for time series forecasting?" in *AAAI Conference on Artificial Intelligence*, vol. 37, no. 9, 2023, pp. 11 121–11 128.
- [49] Z. Xu, A. Zeng, and Q. Xu, "FITS: Modeling time series with 10k parameters," *arXiv preprint arXiv:2307.03756*, 2023.
- [50] S. Huang and Y. Liu, "FL-Net: A multi-scale cross-decomposition network with frequency external attention for long-term time series forecasting," *Knowledge-Based Systems*, p. 111473, 2024.
- [51] R. Yang, L. Cao, J. YANG *et al.*, "Rethinking fourier transform from a basis functions perspective for long-term time series forecasting," *Advances in Neural Information Processing Systems*, vol. 37, pp. 8515–8540, 2024.
- [52] S. Li, X. Jin, Y. Xuan, X. Zhou, W. Chen, Y.-X. Wang, and X. Yan, "Enhancing the locality and breaking the memory bottleneck of transformer on time series forecasting," *Neural Information Processing Systems Conference*, vol. 32, 2019.
- [53] R. Yang, L. Cao, J. Li, and J. Yang, "Variational hierarchical n-beats model for long-term time-series forecasting," *IEEE Transactions on Neural Networks and Learning Systems*, 2025.
- [54] T. Kim, J. Kim, Y. Tae, C. Park, J.-H. Choi, and J. Choo, "Reversible instance normalization for accurate time-series forecasting against distribution shift," in *International Conference on Learning Representations*, 2021.
- [55] O. Ronneberger, P. Fischer, and T. Brox, "U-net: Convolutional networks for biomedical image segmentation," in *MICCAI*. Springer, 2015, pp. 234–241.
- [56] T. Zhang, Y. Zhang, W. Cao, J. Bian, X. Yi, S. Zheng, and J. Li, "Less is more: Fast multivariate time series forecasting with light sampling-oriented mlp structures. arxiv 2022," *arXiv preprint arXiv:2207.01186*, 2022.
- [57] Y. Liu, H. Wu, J. Wang, and M. Long, "Non-stationary transformers: Exploring the stationarity in time series forecasting," *Advances in neural information processing systems*, vol. 35, pp. 9881–9893, 2022.



Xin You received the B.S. degree in Department of Automation from Harbin Institute of Technology, Harbin, China, in 2020. He is currently working towards the Ph.D. degree majoring at the Institute of Image Processing and Pattern Recognition, Department of Automation, Shanghai Jiao Tong University, supervised by Prof. Yun Gu. His research interests include medical image segmentation, video frame interpolation, medical image synthesis.



Kun Fang received the B.S. degree from Tongji University, Shanghai, China, in 2018, and the M.S. and Ph.D. degrees from Shanghai Jiao Tong University, Shanghai, China, in 2021 and 2025, respectively. He is now a postdoctoral fellow at The Hong Kong Polytechnic University. His current research interests include robustness and privacy of deep neural networks.



Runze Yang received the B.S. and M.S. degrees from the Faculty of Mathematical and Physical Sciences, University College London, London, U.K., in 2019 and 2020, respectively. He is a Cotutelle PhD student at both Shanghai Jiao Tong University and Macquarie University. His research interests include multivariate time series forecasting, signal processing, pattern recognition, and machine learning.



Jianxun Li received the Dr. Eng. degree in control theory and engineering with highest honors from Northwestern Polytechnical University, Xi'an, China, in 1996. He is currently a Professor with the Department of Automation, Shanghai Jiao Tong University, Shanghai, China. From 1997 to 1999, he joined the Key Laboratory of Radar Signal Processing of Xidian University, Xi'an, China, as a Postdoctoral Fellow. He was a visiting Professor with the Imperial College London, London, U.K., from 2006 to 2007. His research interests include information fusion, infrared image processing, and parameter estimation.



Longbing Cao (SM'06) received a PhD degree in pattern recognition and intelligent systems at Chinese Academy of Sciences in 2002 and another PhD in computing sciences at University of Technology Sydney in 2005. He is the Distinguished Chair Professor in AI at Macquarie University and an Australian Research Council Future Fellow (professorial level). His research interests include AI and intelligent systems, data science and analytics, machine learning, behavior informatics, and enterprise innovation.



Jie Yang received the bachelor's and master's degrees from Shanghai Jiao Tong University, Shanghai, China, in 1985 and 1988, respectively, and the Ph.D. degree from the University of Hamburg, Hamburg, Germany, in 1994. He is currently a Professor and the Director of the Institute of Image Processing and Pattern Recognition, Shanghai Jiao Tong University. His research interests include image processing, pattern recognition, data mining, and artificial intelligence.

APPENDIX

We provide the proof that the real-valued inverse discrete Fourier transform can be represented by sine and cosine functions as follows:

$$\begin{aligned}
\mathbf{X}[n] &= \frac{1}{T} \sum_{k=0}^{T-1} \mathbf{H}[k] \exp\left(i \frac{2\pi kn}{T}\right) \\
&= \sum_{k=0}^{\frac{T}{2}} \mathbf{H}[k] \left(\cos\left(\frac{2\pi kn}{T}\right) + i \sin\left(\frac{2\pi kn}{T}\right) \right) \\
&\quad + \sum_{k=1}^{\frac{T}{2}-1} \mathbf{H}[T-k] \left(\cos\left(\frac{-2\pi kn}{T}\right) + i \sin\left(\frac{-2\pi kn}{T}\right) \right), \\
&= \frac{1}{T} (\mathbf{H}_{\mathbf{R}}[0] + \mathbf{H}_{\mathbf{R}}[\frac{T}{2}] \cos(\pi n)) \\
&\quad + \sum_{k=1}^{\frac{T}{2}-1} (\mathbf{H}_{\mathbf{R}}[k] + i \mathbf{H}_{\mathbf{I}}[k]) \left(\cos\left(\frac{2\pi kn}{T}\right) + i \sin\left(\frac{2\pi kn}{T}\right) \right) \\
&\quad + \sum_{k=1}^{\frac{T}{2}-1} (\mathbf{H}_{\mathbf{R}}[k] - i \mathbf{H}_{\mathbf{I}}[k]) \left(\cos\left(\frac{2\pi kn}{T}\right) - i \sin\left(\frac{2\pi kn}{T}\right) \right), \\
&= \frac{2}{T} \sum_{k=1}^{\frac{T}{2}-1} \left(\mathbf{H}_{\mathbf{R}}[k] \cos\left(\frac{2\pi kn}{T}\right) - \mathbf{H}_{\mathbf{I}}[k] \sin\left(\frac{2\pi kn}{T}\right) \right) \\
&\quad + \frac{1}{T} (\mathbf{H}_{\mathbf{R}}[0] + \mathbf{H}_{\mathbf{R}}[\frac{T}{2}] \cos(\pi T)), \\
&= \frac{1}{T} \sum_{k=0}^{\frac{T}{2}} \left(a_k \cos\left(\frac{2\pi kn}{T}\right) - b_k \sin\left(\frac{2\pi kn}{T}\right) \right) \\
n &= 0, \dots, T-1, \\
a_k &= \begin{cases} \mathbf{H}_{\mathbf{R}}[k], & k = 0, \frac{T}{2} \\ 2 \cdot \mathbf{H}_{\mathbf{R}}[k], & k = 1, \dots, \frac{T}{2} - 1. \end{cases} \quad b_k = \begin{cases} \mathbf{H}_{\mathbf{I}}[k], & k = 0, \frac{T}{2} \\ 2 \cdot \mathbf{H}_{\mathbf{I}}[k], & k = 1, \dots, \frac{T}{2} - 1. \end{cases}
\end{aligned} \tag{7}$$